OFFICE OF NAVAL RESEARCH

Contract N00014-84-G-0201

Task No. 0051-865

Technical Report #41

Bis(dioxolene)bis(pyridine)ruthenium Redox Series

By

P.R. Auburn, E.S. Dodsworth, M.-A. Haga, W. Liu, W.A. Nevin and A.B.P. Lever*

in

Inorganic Chemistry

York University
Department of Chemistry, 4700 Keele St., North York
Ontario, Canada M3J 1P3

SECURITY CLASSIFICATION OF THIS PAGE

REPORT DOCUMENTATION PAGE

1a. REPORT SECURITY CLASSIFICATION	1b. RESTRICTIVE MARKINGS
2a. SECURITY CLASSIFICATION AUTHORITY Unclassified	3. DISTRIBUTION/AVAILABILITY OF REPORT As it appears on the report
2b. DECLASSIFICATION/DOWNGRADING SCHEDULE	
4. PERFORMING ORGANIZATION REPORT NUMBER(S) Report # 41	5. MONITORING ORGANIZATION REPORT NUMBER(S)
6a. NAME OF PERFORMING ORGANIZATION A.B.P. Lever, York University Chemistry Department (6b. OFFICE SYMBOL (If applicable))	7a. NAME OF MONITORING ORGANIZATION Office of Naval Research
6c. ADDRESS (City, State, and ZIP Code) 4700 Keele St., North York, Ontario M3J 1P3 Canada	7b. ADDRESS (City, State, and ZIP Code) Chemistry Division 800 N. Quincy Street Arlington, VA 22217 U.S.A.
8a. NAME OF FUNDING/SPONSORING ORGANIZATION (8b. OFFICE SYMBOL (If applicable))	9. PROCUREMENT INSTRUMENT IDENTIFICATION NUMBER N00014-84-G-0201
8c. ADDRESS (City, State, and ZIP Code)	10. SOURCE OF FUNDING NUMBERS PROGRAM ELEMENT NO. / PROJECT NO. / TASK NO / WORK UNIT ACCESSION NO

11. TITLE (Include Security Classification)
Bis(dioxolene)bis(pyridine)ruthenium Redox Series

12. PERSONAL AUTHOR(S)
P.R. Auburn, E.S. Dodsworth, M.-A. Haga, W. Liu, W.A. Nevin and A.B.P. Lever*

13a. TYPE OF REPORT	13b. TIME COVERED	14. DATE OF REPORT (Year, Month, Day)	15. PAGE COUNT
Technical	FROM Aug. 90 TO Aug. 91	August 20, 1991	52

16. SUPPLEMENTARY NOTATION

17. COSATI CODES			18. SUBJECT TERMS (Continue on reverse if necessary and identify by block number)
FIELD	GROUP	SUB-GROUP	Ruthenium, Quinone, Pyridine, Electronic Spectra, Electrochemistry

19. ABSTRACT (Continue on reverse if necessary and identify by block number)

A series of ruthenium complexes containing non-innocent, 1,2-dioxolene ligands (dioxolene refers to any of the series catechol-semiquinone-quinone) have been prepared. These have the formula trans-$[Ru(RPy)_2(dioxolene)_2]^n$ where RPy are a series of substituted pyridines and n = -1,0,+1. Their electrochemical and spectroscopic (NMR,ESR,IR,PES, electronic) properties are reported and discussed in terms of their electronic structures, described using simple qualitative molecular orbital models. Their electronic structures are subtly different from those of the related cis-$[Ru(bpy)(dioxolene)_2]^n$ species reported previously (bpy = 2,2'-bipyrdine). The neutral (n=0) complexes have a fully delocalized, mixed valence $Ru^{III}(RPy)_2$(catechol)(semiquinone) electronic structure. The oxidized (n = +1) and reduced (n = -1) species are also Ru^{III} species. The electronic absorption data show a variety of different charge transfer (CT) bands whose assignments are based upon energy variations with change of pyridine and/or dioxolene substituent, and net oxidation state.

20. DISTRIBUTION/AVAILABILITY OF ABSTRACT	21. ABSTRACT SECURITY CLASSIFICATION
☒ UNCLASSIFIED/UNLIMITED ☐ SAME AS RPT ☐ DTIC USERS	Unclassified/unlimited
22a. NAME OF RESPONSIBLE INDIVIDUAL Dr. Ronald A. De Marco	22b. TELEPHONE (Include Area Code) / 22c. OFFICE SYMBOL

DD FORM 1473, 84 MAR 83 APR edition may be used until exhausted
All other editions are obsolete

SECURITY CLASSIFICATION OF THIS PAGE

TECHNICAL REPORT DISTRIBUTION LIST - GENERAL

Office of Naval Research (2)*
Chemistry Division, Code 1113
800 North Quincy Street
Arlington, Virginia 22217-5000

Dr. James S. Murday (1)
Chemistry Division, Code 6100
Naval Research Laboratory
Washington, D.C. 20375-5000

Dr. Robert Green, Director (1)
Chemistry Division, Code 385
Naval Weapons Center
China Lake, CA 93555-6001

Dr. Eugene C. Fischer (1)
Code 2840
David Taylor Research Center
Annapolis, MD 21402-5067

Dr. Elek Lindner (1)
Naval Ocean Systems Center
Code 52
San Diego, CA 92152-5000

Commanding Officer (1)
Naval Weapons Support Center
Dr. Bernard E. Douda
Crane, Indiana 47522-5050

Dr. Richard W. Drisko (1)
Naval Civil Engineering
Laboratory
Code L52
Port Hueneme, CA 93043

Dr. Harold H. Singerman (1)
David Taylor Research Center
Code 283
Annapolis, MD 21402-5067

Chief of Naval Research (1)
Special Assistant for Marine
Corps Matters
Code 00MC
800 North Quincy Street
Arlington, VA 22217-5000

Defense Technical Information
Center (2)
Building 5, Cameron Station
Alexandria, VA 22314

* Number of copies to forward

Enclosure (2)

ABSTRACT DISTRIBUTION LIST

Professor Hector Abruña
Department of Chemistry
Cornell University
Ithaca, NY 14853

Professor C. A. Angell
Arizona State University
Department of Chemistry
Tempe, AZ 85287

Professor Allen Bard
Department of Chemistry
University of Texas at Austin
Austin, TX 78712-1167

Professor Douglas Bennion
Department of Chemical Engineering
350 CB
Birgham Young University
Provo, UT 84602

Professor Lesser Blum
Department of Physics
University of Puerto Rico
Rio Piedras, PUERTO RICO 00931

Professor Daniel Buttry
Department of Chemistry
University of Wyoming
Laramie, WY 82071

Professor Bruce Dunn
Departement of Materials Science and Engineering
University of California, Los Angeles
Los Angeles, CA 90024

Professor Andrew Ewing
Department of Chemistry
152 Davey Laboratory
Pennsylvania State University
University Park, PA 16802

Professor Gregory Farrington
University of Pennsylvania
Department of Materials Science and Engineering
3231 Walnut Street
Philadelphia, Pennsylvania 19104

Professor W. R. Fawcett
Department of Chemistry
University of California, Davis
Davis, CA 95616

Professor Harry Gray
California Institute of Technology
127-72
Pasadena, California 91125

Professor Joel Harris
Department of Chemistry
University of Utah
Salt Lake City, UT 84112

Professor Adam Heller
Department of Chemical Engineering
University of Texas at Austin
Austin, TX 78712-1062

Professor Pat Hendra
The University
Southampton SO9 5NH
ENGLAND

Professor Joseph Hupp
Department of Chemistry
Northwestern University
Evanston, IL 60208

Professor Jiri Janata
Department of Bioengineering
University of Utah
Salt Lake City, UT 84102

Professor A. B. P. Lever
Department of Chemistry
York University
4700 Keele Street
North York, Ontario M3J 1P3

Professor Nathan S. Lewis
Division of Chemistry and Chemical Engineering
California Institute of Technology
Pasadena, CA 91125

Professor Rudolph Marcus
Division of Chemistry and Chemical Engineering
California Institute of Technology
Pasadena, CA 91125

Professor Charles Martin
Department of Chemistry
Colorado State University
Ft. Collins, CO 80523

Professor Royce W. Murray
Department of Chemistry
University of North Carolina at Chapel Hill
Chapel Hill, NC 27514

Dr. Michael R. Philpott
IBM Research Division
Almaden Research Center
650 Harry Road
San Jose, CA 95120-6099

Professor B. S. Pons
Department of Chemistry
University of Utah
Salt Lake City, UT 84112

Dr. Debra Rolison
Code 6170
Naval Research Laboratory
Washington, DC 20375-5000

Professor Donald Schleich
Department of Chemistry
Polytechnic University
333 Jay Street
Brooklyn, NY 11201

Professor Jack Simons
Department of Chemistry
University of Utah
Salt Lake City, UT 84112

Dr. H. Gilbert Smith
TSI Mason Research Institute
57 Union Street
Worcester, MA 01608

Professor Eric Stuve
Department of Chemical Engineering, BF-10
University of Washington
Seattle, WA 98195

Dr. Stanislaw Szpak
Code 634
Naval Ocean Systems Center
San Diego, CA 92152-5000

Professor Petr Vanýsek
Department of Chemistry
Northern Illinois University
Dekalb, IL 60115

Professor Michael Weaver
Department of Chemistry
Purdue University
West Lafayette, IN 49707

Professor Henry White
Department of Chem. Eng. and
Materials Science
421 Washington Ave., SE
University of Minnesota
Minneapolis, MN 55455

Professor. Mark Wightman
Department of Chemistry
University of North Carolina
Chapel Hill, NC 27599-1350

Professor George Wilson
Department of Chemistry
University of Kansas
Lawrence, KS 66045

Professor Mark S. Wrighton
Department of Chemistry
Massachusetts Institute of Technology
Cambridge, MA 02139

Professor Ernest Yeager
Case Center for Electrochemical Sciences
Case Western Reserve University
Cleveland, OH 44106

Contribution from the Department of Chemistry, York University, North York, Ontario, Canada, M3J 1P3.

Bis(dioxolene)bis(pyridine)ruthenium Redox Series

Pamela R. Auburn,[1a] Elaine S. Dodsworth, Masa-Aki Haga,[1b] Wei Liu,[1c] W. Andrew Nevin[1d] and A. B. P. Lever*

Abstract

A series of ruthenium complexes containing non-innocent 1,2-dioxolene ligands (dioxolene refers to any of the series catechol-semiquinone-quinone) have been prepared. These have the formula trans-$[Ru(RPy)_2(dioxolene)_2]^n$ where RPy are a series of substituted pyridines and n = -1,0,+1. Their electrochemical and spectroscopic (NMR, ESR, IR, PES, electronic) properties are reported and discussed in terms of their electronic structures, described using simple qualitative molecular orbital models. Their electronic structures are subtly different from those of the related cis-$[Ru(bpy)(dioxolene)_2]^n$ species reported previously (bpy = 2,2'-bipyridine). The neutral (n = 0) complexes have a fully delocalized, mixed valence $Ru^{III}(RPy)_2$(catechol)(semiquinone) electronic structure. The oxidized (n = +1) and reduced (n = -1) species are also Ru^{III} species. The electronic absorption data show a variety of different charge transfer (CT) bands whose assignments are based upon energy variations with change of pyridine and/or dioxolene substituent, and net oxidation state.

Introduction

1,2-Dioxolenes, members of the catechol-semiquinone-quinone redox chain, have orbitals which are close in energy to the transition metal d orbitals. The charge distribution in dioxolene coordination complexes depends upon the relative energies and overlap of these metal and dioxolene ligand orbitals.[2,3] In general, the energies are sufficiently disparate that the metal and dioxolene levels remain discrete within the electronic structures of these complexes. This is in sharp contrast to the closely related dithiolene ligands which form complexes characterized by extensive electron delocalization.[4,5] We recently reported studies of redox series based upon the $Ru(bpy)_2$(dioxolene) and Ru(bpy)$(dioxolene)_2$ species (bpy = 2,2'-bipyridine), and provided evidence for the first highly delocalized dioxolene complexes.[6-9] Similar behaviour has also been demonstrated for related osmium complexes[10] and Ru$(dioxolene)_3$.[11]

We now report a series of analogous trans-$Ru(RPy)_2(R'Diox)_2$ complexes (Chart I). These species are more amenable to synthetic variation, and thus allow a systematic study of the factors influencing the electronic structures of these materials. The bis(pyridine) complexes are initially isolated in the trans geometric configuration, but can be isomerized readily to cis. The kinetic and mechanistic aspects of this isomerization will be reported separately.[12]

Chart I

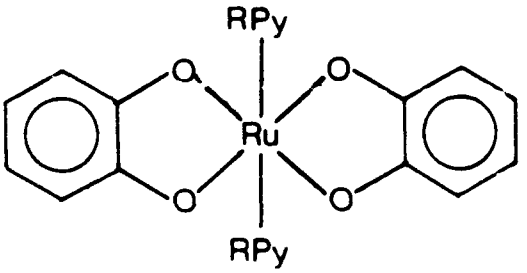

In the discussion which follows, the abbreviation R'Diox is used for a dioxolene of unspecified oxidation state, while the abbreviations q, sq and cat are used to specify the quinone, semiquinone and catechol oxidation states. Thus for instance, DTBDiox is a general term for DTBCat, DTBSq or DTBQ. As in the previous study,[9] the symbol S is used for the initially

derived starting material, and **O1**, **O2**, **R1** and **R2** are used for the first and second oxidized and first and second reduced species respectively. The symbols c and t designate cis and trans isomers.

Experimental

Methods. Electronic spectra in the visible and near infrared (NIR) were recorded with a Perkin Elmer microprocessor model 340 spectrometer. Fourier transform infrared (FTIR) data were obtained using a Nicolet SX20 spectrometer. Samples were prepared as KBr pellets or as Nujol or hexachlorobutadiene (HCBD) mulls. NMR spectra were obtained using a Bruker AM 300 FT NMR spectrometer. Photoelectron spectra (PES) were collected by the Surface Science Centre at the University of Western Ontario, London, Ontario. Magnetic data were obtained, courtesy of Professor L.K. Thompson (Memorial University, Newfoundland), using a Faraday magnetometer (see ref. 13 for details). Electron spin resonance (ESR) spectra were obtained using a Varian E4 spectrometer, and were calibrated against diphenylpicrylhydrazide (DPPH).

Electrochemical data were collected with a Princeton Applied Research (PARC) model 173 potentiostat, or a PARC model 174 Polarographic Analyser, coupled to a PARC model 175 Universal Programmer. Cyclic and differential pulse voltammetry were carried out using platinum wires as working and counter electrodes, and a AgCl/Ag quasi-reference electrode with ferrocene (Fc) as an internal standard. The Fc^+/Fc couple was assumed to lie at +0.425 V vs SCE;[14] this appears to be a more realistic value than those cited in our earlier work.[6,9] Spectroelectrochemical experiments utilized a modified 1 cm glass cuvette equipped with a AgCl/Ag reference electrode, a Nichrome wire counter electrode and a platinum gauze working electrode. The reference and counter electrodes were each separated from the bulk solution by a sintered glass frit.

Materials. Tetrabutylammonium perchlorate (TBAP, Kodak) and tetrabutyl ammonium hexafluorophosphate (TBAH, Aldrich) were recrystallized from absolute ethanol and dried in a vacuum oven at 50° C for 2 d. o-Dichlorobenzene (DCB, Aldrich Gold Label) was used as supplied. 1,2 dichloroethane (DCE, BDH Omnisolve) was dried and distilled from P_2O_5.

Dichloromethane (DCM, BDH Analytical) was dried over CaH_2, and diethyl ether over $LiAlH_4$, and both were distilled under nitrogen prior to use. 3,5-Di-tert-butylcatechol ($DTBCatH_2$, Aldrich) and 4-butyl catechol ($TBCatH_2$, Aldrich) were recrystallized from ethanol. Catechol ($CatH_2$), 4-methylcatechol ($MeCatH_2$) and 4-chlorocatechol ($ClCatH_2$) were obtained from Tokyo Kasei and used as supplied. Pyridine and pyridine derivatives (Aldrich) were distilled or recrystallized prior to use. 4-Chloropyridine hydrochloride (Aldrich) was used as supplied. Cobaltocene (Cp_2Co, Strem) was sublimed prior to use. Silver salts, $AgClO_4$, $AgSO_3CF_3$ and $AgPF_6$ (Aldrich), were used as supplied. $[Ru_2(OAc)_4Cl]_n$ was prepared according to a published procedure.[15]

Preparation of Complexes.

t-Ru(Py)$_2$(DTBDiox)$_2$. (DTBDiox is derived from 3,5-di-t-butylcatechol) To a boiling mixture of $[Ru_2OAc_4Cl]_n$ (0.4 g, 0.84 mmol) and $DTBCatH_2$ (0.753 g, 3.39 mmol) in methanol (50 mL) under nitrogen was added a solution of NaOH (0.27 g, 6.77 mmol) in methanol (15 mL). The solids dissolved to give a deep purple solution to which, after 1 h, pyridine (1 mL) was added. After refluxing for an additional 5 h, the resultant orange-brown solution was exposed to the atmosphere and filtered. During this procedure the solution became blue-green in color. The filtrate was allowed to cool and then stand at ambient temperature for 12 h. Black-green needles of the product were isolated by filtration, washed with methanol and air-dried.

t-Ru(RPy)$_2$(R'Diox)$_2$. (RPy is 3- or 4-acetylpyridine (3-AcPy, 4-AcPy), 3- or 4-chloropyridine (3-ClPy, 4-ClPy), 3- or 4-phenylpyridine (3-PhPy, 4-PhPy), 4-vinylpyridine (4-VPy), 4-picoline (4-MePy), 3- or 4-ethylpyridine (3-EtPy, 4-EtPy) or 4-butylpyridine (4-BuPy), and R'Diox is derived from 3,5-di-t-butylcatechol, 4-t-butylcatechol, 4-methylcatechol, catechol or 4-chlorocatechol) These complexes were prepared, using the appropriate ligand partners, following the procedure above. When the 4-ClPy ligand was required it was generated <u>in situ</u> from the hydrochloride by use of an additional stoichiometric amount of base in the above procedure. The solubilities of the reaction products varied. Filtrates containing 3-AcPy or 4-AcPy complexes required concentration before the product would crystallize, whereas complexes containing the

4-PhPy or 3-PhPy ligands precipitated from the hot reaction mixtures before filtration. Products so isolated, washed with methanol and air dried were found to be pure. Yields were between 10 and 40%. Analytical data and yields are given as supplementary material (Table SI).

t-[Ru(3-ClPy)$_2$(DTBDiox)$_2$]ClO$_4$. To a stirred solution of t-Ru(3-ClPy)$_2$(DTBDiox)$_2$ (46.2 mg, 0.06 mmol) in dry dichloromethane (10 mL), under nitrogen, was added dropwise a solution of $AgClO_4$ (12.5 mg, 0.06 mmol) in acetonitrile (1 mL). During the addition, the solution changed in color from yellow-green to blue. The mixture was stirred at ambient temperature for 3 h. The precipitated metallic silver was removed by filtration through a short plug of Celite. The filtrate was concentrated under reduced pressure and diethyl ether was added to initiate crystallization. The mixture was stored at -5^{o}C for 72 h. Dark blue crystals of the product (41.5 mg, 78%) were isolated by filtration, washed with diethyl ether and air-dried.

t-[Ru(RPy)$_2$(R'Diox)$_2$]X. ($X^- = ClO_4^-$, PF_6^- or $SO_3CF_3^-$): These compounds were prepared by analogous procedures using the appropriate ruthenium complex and silver salt. The solubilities of the reaction products varied slightly and occasionally a mixture of diethyl ether and hexanes, or hexanes alone, was required to initiate crystallization. The yields for these reactions varied between 75 and 95%. Analytical data are given in Table SII (supplementary material). For spectroscopic purposes, some of these **O1** materials were generated <u>in situ</u> by the addition of the appropriate silver salt to a solution of the ruthenium **S** complex. Solutions prepared in this manner were filtered prior to spectroscopic measurements.

[Cp$_2$Co][Ru(3-ClPy)$_2$(DTBDiox)$_2$]. This reaction was carried out in a Vacuum Atmospheres dry box. To cobaltocene (40.5 mg, 0.27 mmol) was added a solution of Ru(3-ClPy)$_2$(DTBDiox)$_2$ (150 mg, 0.19 mmol) in dichloromethane (10 mL). A dark green solid precipitated from the resultant mauve solution. The mixture was stirred for about 30 min. to digest the precipitate, and the solid was then allowed to settle (2 h). Dark green crystals (122 mg, 67%) were isolated by filtration, washed sequentially with dichloromethane, diethyl ether and hexanes, and dried <u>in vacuo</u>. (Anal. Calcd. for $RuCoC_{48}H_{58}Cl_2N_2O_4$: C, 60.19; H, 6.10; N, 2.92. Found:

C, 59.67; H, 6.02; N, 2.90%).

For spectroscopic measurements this and other **R1** species were prepared in situ by reduction of the appropriate ruthenium **S** complex with cobaltocene. For ESR experiments the best results were obtained using a slight deficiency of cobaltocene to ensure that the cobaltocene signal did not interfere with the spectrum of the reduced ruthenium complex.

Some representative colors of solutions are as follows:

	R1	**S**	**O1**
$Ru(Py)_2(DTBDiox)_2$	yellow-brown	yellow-green	deep blue
$Ru(4\text{-}BuPy)_2(ClDiox)_2$	yellow-green	violet	blue-green

Results

The starting materials, **S**, and the one-electron oxidized species, **O1**, are air-stable, crystalline solids. The crystal structures of one **S** and one **O1** species have been reported,[7,16,17] and are discussed below. Both possess a trans C_{2h} structure in which the two pyridine planes are parallel and bisect the plane containing the dioxolene ligands. One example of the air-sensitive one-electron reduction product, **R1**, was also isolated in the solid state.

Nuclear Magnetic Resonance Spectra. ^1H NMR data for the even electron starting materials, **S**, are given in Table I. The ^1H NMR spectra are sharp and are temperature-invariant between -60°C and +60°C. The DTBDiox complexes give ^1H and ^{13}C NMR spectra consistent with the presence of only one trans isomer in solution. Solutions of $Ru(3\text{-}ClPy)_2(TBDiox)_2$, $Ru(4\text{-}PhPy)_2(TBDiox)_2$ and $Ru(4\text{-}VPy)_2(TBDiox)_2$ all each show a single t-butyl resonance in the aliphatic spectral region of their ^1H NMR spectra but show two doublets of doublets around 6 ppm due to the protons in the 5-positions of the 4-t-butyldioxolene ligands. Selective decoupling of each individual doublet of doublets in the spectrum of $Ru(4\text{-}VPy)_2(TBDiox)_2$ resulted in the collapse of the doublets due to protons in the 3- and 6-positions of the corresponding isomer.

Magnetism and Electron Spin Resonance. The starting materials (**S**) are diamagnetic on

the basis of their NMR spectra and ESR-silence at room temperature or 77 K (solution and solid state). Magnetic measurements on an **O1** complex, $[Ru(4\text{-}MePy)_2(DTBDiox)_2]ClO_4$, show one unpaired electron. This complex shows Curie-Weiss behaviour (equation of line $\chi_M(corr) = 0.376/(T + 7.81)$; R = 0.998) and has magnetic moments of 1.74 and 1.54 BM at 295 and 5.65 K respectively.

The ESR spectra of the S = 1/2, **O1** and **R1** species, at room temperature, in solution or the solid state, are either broad with g values close to 2, or are undetectable. Signals are observed for all of these species at low temperatures, 77-115 K (Tables II, III, Figure 1). The **O1** signals, in frozen DCE solutions, are broad and centered near the free radical value of g = 2. Frozen DCE solutions of the **R1** species exhibit highly anisotropic signals with two or three distinct g values.

Electrochemistry. The electrochemical behaviour of these species is very similar to that of the $Ru(bpy)(R'Diox)_2$ complexes. Redox chains containing five members may be characterized by cyclic voltammetry of the starting materials (Table IV). The bulk solution rest potentials lie between couples **II** and **III** (Figure 2). The variations of the redox potentials as functions of the pyridine and dioxolene substituents, using the Hammett σ parameters, are shown in Figure 3.

Couples **I-III** are reversible ($i_p \propto v^{1/2}$, $i_c/i_a = 1$) for all species, with peak to peak separations of 65-85 mV at 100 mV s^{-1} in DCE. Couple **IV** is normally quasi-reversible or approaching irreversibility ($i_c/i_a > 1$) but always has a clear return wave. Coulometry was carried out for some couples. On the basis of this and similarities in current from one couple to another all the redox processes involve one electron.

The **R1** and **O1** species may also be generated by bulk electrolysis or by chemical reduction or oxidation respectively. These processes are fully reversible. The **O2** species is unstable on the controlled potential time scale, and attempts to generate it by bulk electrolysis resulted in some decomposition. Attempts to generate **R2** by similar methods resulted in completely irreversible changes.

Fourier Transform Infrared Spectra. FTIR data were collected for most of the S and

O1 complexes (supplementary data, Tables SIII, SIV), and for $[Cp_2Co][Ru(3\text{-}ClPy)_2(DTBDiox)_2]$, the only isolated **R1** material. Spectra of the **O1** species were recorded as Nujol or HCBD mulls since KBr reduces these complexes.

The spectrum of $[Cp_2Co][Ru(3\text{-}ClPy)_2(DTBDiox)_2]$ shows prominent absorptions at 1414, 1404, 1281 and 1237 cm^{-1}. The FTIR spectra of the **S** species are distinguished by intense absorptions around 1150 cm^{-1}, which are unique to this redox level. The spectra of the **O1** species are dominated by counterion absorptions, with other strong bands around 1600 (4-RPy), 1450, 1420, 1370 and 1240 cm^{-1}.

Photoelectron Spectra. Data for the $Ru(3d_{5/2})$ and for the core levels of oxygen and nitrogen are given in Table V.

Electronic Spectra. Solution electronic spectroscopic data for the **R1**, **S**, and **O1** species are collected in Tables VI - VIII and typical spectra are displayed in Figure 4. Representative **S** and **O1** spectra were also obtained in the solid state (as Nujol mulls); these showed no significant differences from the solution data.

Discussion

Stereochemistry. In the trans-$Ru(RPy)_2(DTBDiox)_2$ complex geometry, two 3,5-di-t-butyldioxolene ligands can theoretically give rise to two isomers, one each of C_{2v} and C_{2h} symmetry, depending on the relative orientations of the t-butyl groups (and assuming axial trans ligands). The NMR spectra indicate that only one isomer is formed and the temperature-invariance of these spectra suggests that isomerization does not occur in the temperature range studied. Careful spectroscopic and chromatographic examination of the mother liquors from which these complexes were isolated gave no evidence of a second isomer. This, in concert with the arguments below, suggests that for the bis(3,5-di-t-butyldioxolene) complexes only one trans isomer is formed in the synthetic procedure. Trans to cis isomerization occurs at higher temperatures[12].

Single crystal X-ray data for t-Ru(4-BuPy)$_2$(DTBDiox)$_2$ and t-[Ru(3-ClPy)$_2$(DTBDiox)$_2$]PF$_6$ establishes that the solid state geometry is C_{2h}.[7,16,17] Assuming that the solid state and solution structures are the same, the absence of the C_{2v} isomer may be attributed to an unfavorable steric interaction between the two cis t-butyl substituents in this geometry. Support for this analysis derives from studies of the corresponding mono-substituted, 4-t-butyldioxolene complexes. In these cases, neither trans isomer is likely to be sterically constrained, and ^{1}H NMR data indicate the presence of two isomers. The relative proportions of the two isomers vary (Table I); Ru(4-VPy)$_2$(TBDiox)$_2$ and Ru(4-PhPy)$_2$(TBDiox)$_2$ give the two isomers in approximately equal concentrations, whereas Ru(3-ClPy)$_2$(TBDiox)$_2$ gives an isomer ratio of approximately 3:1.

Electronic Structure. Each of the starting materials gives rise to five redox products as established by cyclic voltammetry (Table IV). Cis-[12] and trans-Ru(RPy)$_2$(R'Diox)$_2$ analogues give distinct, though very similar, cyclic voltammograms. This, and the reversibility of the spectroelectrochemical experiments for the trans species, suggests that no structural changes occur during the redox processes generating **O1** and **R1**, though some decomposition is evident on the longer time scale for **O2** and **R2**.

As discussed previously for the Ru(bpy)(R'Diox)$_2$ complexes,[9] the electronic structures of the various redox products are not obvious from their molecular formulae. Critical evaluation of the possible electronic structures gave the following valence bond descriptions for the various redox species for [Ru(bpy)(R'Diox)$_2$]$^{n+}$, based upon their chemical and physical properties; the first canonical form is believed to be the dominant one. Mixed valence species are delocalized.

Chart II

R2 $[Ru^{II}(bpy)(cat)_2]^{2-}$

R1 $[Ru^{III}(bpy)(cat)_2]^- \text{<===>} [Ru^{II}(bpy)(cat)(sq)]^-$

S $Ru^{II}(bpy)(sq)_2 \text{ <===> } Ru^{III}(bpy)(cat)(sq)$

O1 $[Ru^{II}(bpy)(q)(sq)]^+ \text{ <===> } [Ru^{III}(bpy)(sq)_2]^+$

O2 $[Ru^{II}(bpy)(q)_2]^{2+}$

The electronic structures required to describe the **R1**, **S** and **O1** species were reconciled by a simple molecular orbital model, involving the three ruthenium d (t_{2g} in O_h symmetry) and the dioxolene $3b_1$ (in C_{2v} symmetry) orbitals, which all mix extensively.

Neglecting the ligand substituents, the trans complexes have D_{2h} symmetry. The $3b_1$ (in local C_{2v} symmetry) orbitals[19] of the two dioxolene ligands transform as $b_{1u} + b_{2g}$. The t_{2g} (in local O_h symmetry) orbitals of the central ruthenium atom transform as $a_g + b_{2g} + b_{3g}$. Within this model, the ligand and metal valence orbitals of b_{2g} symmetry mix, while the remaining ligand and metal valence levels remain essentially unmixed. An effective oxidation state of the ruthenium may be calculated by summing the percentage of metal character of each orbital multiplied by its occupancy. The dioxolene lone-pair and pyridine π^* levels are also relevant to a full spectroscopic analysis of these species (Figure 5). The electrochemical and spectroscopic data, for the various redox products, are interpreted in the light of this model using methods discussed in detail elsewhere.[6,8,9]

R2 Species. In the **R2** products, the five valence orbitals are occupied by ten electrons, six from the central ruthenium ion and two from each dioxolene ligand. Thus, regardless of the relative ordering or metal-ligand coefficients of the five valence orbitals, the only possible electronic description for the **R2** complexes is $[Ru^{II}(RPy)_2(cat)_2]^{2-}$. However, since these species are unstable, there is no experimental corroboration of this assignment.

R1 Species. The **R1** complexes have a total of nine valence electrons, with one electron in the highest occupied molecular orbital (HOMO). The character of the HOMO defines the electronic description of these materials. A $[Ru^{III}(RPy)_2(cat)_2]^-$ structure results if the HOMO is predominantly metal, while a $[Ru^{II}(RPy)_2(cat)(sq)]^-$ structure pertains if the HOMO is predominantly ligand in character.

The various **R1** t-$[Ru(RPy)_2(R'Diox)_2]^-$ species have ESR spectra (Table II) with two or three distinct g values, typical of low spin d^5 Ru^{III}.[20-25] While the **R1** $[Ru(bpy)(R'Diox)_2]^-$

species also show evidence for a Ru^{III} contribution,[9] it is certainly not so evident as in these trans-pyridine species.

The Ru^{III} electronic structure requires that both dioxolene ligands be in the catechol oxidation state. This assignment is supported by the IR data for $[Cp_2Co][Ru(3\text{-}ClPy)_2(DTBDiox)_2]$ in which the two strongest bands are at 1237 and 1281 cm^{-1}. Coordinated catechols typically display one or two intense absorptions in the 1250 cm^{-1} region,[26-30] the more intense of which is normally attributed to the C-O stretching mode.

The PES $Ru(3d_{5/2})$ binding energy for $[Cp_2Co][Ru(3\text{-}ClPy)_2(DTBDiox)_2]$ (Table V) is 281.4 eV, in the range which may be associated with either Ru^{II} or Ru^{III}.[31-38] It is higher than the values observed for **R1** species in the bipyridine species[9] and notably higher than the values for S species. While the inner shell binding energies of metals in complexes may be used to infer the oxidation state of the metal, the practice requires caution,[34] and comparisons are best made with complexes containing similar ligands. However the data are consistent with a Ru^{III} species bound to two strongly π-donating catecholate ligands.

Further support for the $[Ru^{III}(RPy)_2(cat)_2]^-$ structure comes from comparison of the shifts in the various redox potentials as a function of pyridine or dioxolene substituent (Figure 3). Couple **IV** is markedly dependent on pyridine substituent whereas couples **I, II** and **III** vary very little, but show a much greater dependence on dioxolene substituent than does couple **IV**. This suggests that couple **IV** is metal-based ($Ru^{III/II}$) and couples **I, II** and **III** are largely dioxolene ligand-based.

Thus the data unequivocally support the formulation $[Ru^{III}(RPy)_2(cat)_2]^-$ and it remains to demonstrate that the electronic spectra (Figure 4, Table VI) can be assigned in this context. The HOMO, $2b_{2g}^*$, is then mainly metal and the lower energy electronic transitions will terminate thereon.

The lowest energy absorption (band (**R1,I**)) occurring between 800 and 850 nm is clearly attributable to a catechol (π) to ruthenium (dπ) ligand to metal charge transfer (LMCT) transi-

tion,[39] b_{1u} ---> $2b_{2g}^*$, as seen in other catechol complexes containing reducible metal ions.[25,30,40-42] It shifts to the blue as the catechol becomes, upon substitution, a weaker donor, and shifts to the red with decreasing basicity of the pyridine ligand. Moreover band (**R1,I**) tracks the potential of the $Ru^{III/II}$ redox couple, **IV**, for the series of DTBDiox complexes. The correlation is linear, with a small negative slope (1), i.e. a blue shift in the LMCT transition as the Ru^{III} species becomes more difficult to reduce (Figure 6).

Band (**R1,I**): $\nu\ (cm^{-1}) = -3450\ E(Ru^{III/II}) + 6550$ (R = 0.95, 11 pts.) (1)

Strictly, this type of correlation is only valid for a reversible redox couple, which is not the case for couple **IV**.[43] However the deviations from reversibility are not very large.

In the visible region there are two absorptions (bands (**R1,II,III**)) which might be attributed to pyridine (π) to Ru($d\pi$) LMCT transitions.[44] However bands (**R1,II,III**) cannot be assigned in this manner since they both shift substantially to the red as the pyridine ligand becomes a better electron acceptor, and to the blue as the R'Diox becomes a poorer donor. This behaviour indicates metal to ligand charge transfer (MLCT) involving pyridine, or a second cat ---> Ru($d\pi$) LMCT (from a lower catechol orbital), or possibly a cat ---> RPy ligand to ligand charge transfer (LLCT) transition. The higher sensitivity of these bands to pyridine substitution relative to band (**R1,I**), and the lack of a second LMCT band in other catechol complexes,[45,46] suggests that the LMCT assignment is not appropriate. We propose that these are MLCT transitions even though the metal is Ru^{III}. They occur in the visible region because of the very negative $Ru^{III/II}$ potential, **IV**. Two MLCT transitions to pyridine are allowed by symmetry (Figure 5), Ru(a_g,$2b_{2g}^*$) ---> RPy(b_{3u}^*). These are assigned to bands (**R1,II**) and (**R1,III**) respectively as the latter is expected to be stronger due to better overlap. LLCT transitions, b_{2g} ---> b_{3u}^* and b_{1u} ---> $3b_{2g}^*$, may also contribute to intensity in this region.

For the DTBDiox complexes both transitions (**R1,II,III**) track the $Ru^{III/II}$ potential with significantly larger negative slopes than for the 800 nm absorption (Figure 6). The correlations are

rather scattered, probably because many of the transitions appear as shoulders whose true transition energies are difficult to define accurately. These transitions for the 4-vinyl- and 4-phenylpyridine complexes lie well below the correlation lines and are not included in the statistics in (2,3). The extra red shift for these last two species results from conjugation of the pyridine π system with that of the substituent, which lowers the π^* level while not affecting the donor properties of the pyridine ligand, and thus lowers the MLCT energy. This is further evidence for the MLCT (or LLCT) assignment.

Band (**R1,II**): $\nu\ (cm^{-1}) = -11700\ E(Ru^{III/II}) + 446$ (R = 0.95, 7 pts.) (2)

Band (**R1,III**): $\nu\ (cm^{-1}) = -15700\ E(Ru^{III/II}) + 1870$ (R = 0.82, 7 pts.) (3)

Note that it would be more appropriate to correlate the MLCT transitions with the $Ru^{IV/III}$ potentials but these data are not available; there is little doubt however that the $Ru^{III/II}$ potential (IV) varies with pyridine substituent in a parallel manner to the $Ru^{IV/III}$ potential.[47]

Band (**R1,IV**) occurs in most cases as a shoulder on the rising ligand UV absorption and its behaviour with changing substituents is not clear. It is almost certainly a CT transition as the ligands do not absorb at this energy.

S Species. The single crystal X-ray structure[7,16] of t-$Ru(4\text{-}BuPy)_2(DTBDiox)_2$ does not clearly define the electronic structure of this complex. The C-O bond lengths of coordinated dioxolenes are normally characteristic of the ligand oxidation state.[2,48] However, this species shows average dioxolene C-O bond lengths of about 1.32 Å, identical to those in $Ru(bpy)(Diox)_2$ and significantly longer than those usually associated with coordinated semiquinones (1.29 Å) but shorter than the 1.35-1.37 Å expected for coordinated catechols. Also similarly to $Ru(bpy)(Diox)_2$, the dioxolene rings have only very slight quinonoid character. The two dioxolene ligands are equivalent, although thermal disorder cannot absolutely be ruled out.

The ruthenium-oxygen bond lengths average 1.994 Å, 0.05 Å shorter than the Ru-O bonds

in $[Ru^{II}(bpy)_2(DTBSq)]^+$,[16] and also shorter than the 2.028 Å average Ru-O bond length of $[Ru^{III}(C_2O_4)_3]^{3-}$,[49] but longer than the average Ru-O distance of 1.97 Å in $Ru(DTBDiox)_3$.[11] The Ru-N bonds are 2.08 Å, longer than those in either $[Ru^{II}(bpy)_2(DTBSq)]^+$ or $[Ru(bpy)_3]^{2+}$.[16,50] These data are consistent with a $Ru^{III}(RPy)_2(cat)(sq)$ delocalized mixed valence electronic structure.

The electrochemical data also support this view. Although the HOMO in **R1** has mainly metal character, the large variation in redox potential **III** with dioxolene substituent (and relatively small variation with pyridine substituent (Figure 3)) indicates that **R1** and **S** differ by one dioxolene ligand-based electron in their electronic structures, giving $Ru^{III}(RPy)_2(cat)(sq)$. However, the PES data (Table V) for several **S** complexes show $Ru(3d_{5/2})$ binding energies well within the normal Ru^{II} range,[31-38] and lower than that observed for $[Ru^{III}(3\text{-}ClPy)_2(DTBDiox)_2]^-$. This observation rules out the possibility of Ru^{IV} but suggests that there is some contribution from a Ru^{II} canonical form, similar to the situation in $Ru(bpy)(R'Diox)_2$. The diamagnetism of the **S** complexes requires that the Ru^{III} and sq in the mixed valence structure be strongly antiferromagnetically coupled.

As previously observed for cis-$Ru(bpy)(R'Diox)_2$ and $Ru(DTBDiox)_3$ complexes,[9,11] the FTIR spectra of the trans-**S** species containing DTBDiox are dominated by a strong absorption at about 1150 cm^{-1}, which is not typical of either catechol or semiquinone species,[26-30] though a similar band has been reported in a series of Cu^{II}-semiquinone complexes.[51] The intensity of this absorption is convincing evidence that, despite its unusual position, it is associated with a C-O stretching vibration of the dioxolene ligand. Other IR absorptions are fairly typical of coordinated semiquinone and there is no evidence for localized cat and sq ligands on the vibrational time-scale.

A localized mixed valence system, which is unlikely in view of the strong Ru^{III}-sq coupling, is expected to show a broad cat ---> sq transition in the NIR region, as seen in analogous Cr, Fe and Co complexes.[29,52,53] A band is observed in this region (see below) but it is extremely intense and narrow, indicative of strongly coupled, Class III, mixed valence behav-

iour.[54] Strong coupling requires a strong interaction between the ligand and metal b_{2g} orbitals as the ligands are too far apart to overlap directly. The anti-bonding combination, $2b_{2g}^*$, will be the lowest unoccupied molecular orbital (LUMO) (Figure 5). If this were mainly metal b_{2g}, then the formal structure would approach $Ru^{IV}(RPy)_2(cat)_2$, while if it were dominantly ligand, it would be $Ru^{II}(RPy)_2(sq)_2$; a 50-50 mixed orbital leads to a Ru^{III} electronic structure with fully delocalized ligands. Most of the experimental data indicate that the Ru^{III} formula is the closest to reality, but the PES and IR spectra suggest that there is some $Ru^{II}(RPy)_2(sq)_2$ character, and therefore we conclude that the LUMO b_{2g}^* orbital has slightly more than 50% ligand character.

The electronic spectra (Figure 4) of these materials are dominated by the intense NIR absorption (band (**S,I**)) centered at about 1150 nm. Unlike band (**R1,I**), this transition is essentially unaffected by changing the pyridine substituent. There is a small dependence (Table VII) upon dioxolene substituent, the band shifting to higher energy for the less electron-donating dioxolenes, in accordance with an LMCT dioxolene ---> Ru(dπ) assignment. This behaviour is appropriate for a b_{1u} ---> $2b_{2g}^*$ excitation which is a bis(dioxolene) transition with LMCT character developed to the extent that the b_{2g} orbital has metal character. Typically, the NIR band has a high energy shoulder which may be a vibronic band as the splitting is small, typically around 400 cm^{-1}, possibly corresponding to ν(Ru-O).

Since the HOMO is the filled b_{1u} orbital and the LUMO is the even $2b_{2g}^*$, few transitions are allowed in this system, accounting for the absence of strong bands in the visible region. The broad, weak absorption near 580 nm (band (**S,II**)) is affected by ligand substituents in a similar manner to the NIR band. This may be the dioxolene n ---> π^* transition which occurs around 700 nm in free semiquinones.[55] The highest dioxolene lone pair orbitals ($9a_1$ in the free ligand[19]) transform as $a_g + b_{3u}$ in D_{2h} symmetry. The 580 nm band is therefore assigned to b_{3u} ---> $2b_{2g}^*$ which is overlap forbidden, explaining its weakness. Preliminary resonance Raman data show no involvement of the axial pyridine ligands in this transition.[56]

Bands (**S,III**) are assigned to Ru(dπ) ---> RPy(π^*) MLCT transitions which are expected

in the near UV, higher in energy than in the **R1** species because the available d electrons are stabilized in S. Two transitions are seen in this region for complexes with the more electron-withdrawing pyridine substituents and these transitions move to particularly low energy with the conjugated 4-phenyl and 4-vinyl substituents, as discussed above for **R1**. Preliminary resonance Raman data confirm the involvement of pyridine in this region.[56] Band (**S,IV**), around 320 nm, varies little with pyridine substituent and is assigned to the dioxolene π ---> π^* transition (involving $2b_{2g}{}^*$) which occurs at 380 nm in most semiquinone complexes.[55]

O1 Species. X-ray analysis[17] of $[Ru(3\text{-}ClPy)_2(DTBDiox)_2]^+$ shows clearly that both dioxolene ligands are in the semiquinone oxidation state and therefore the metal is Ru^{III}. The average dioxolene C-O distance is 1.29 Å which is typical of semiquinones.[2,48] The Ru-O and Ru-N distances are both slightly longer than those in the **S** species and the dioxolenes clearly have quinonoid character. The increase in metal-ligand bond lengths may be due to loss of π backbonding capability which exists in **S** because of the Ru^{II} character.

The $[Ru^{III}(RPy)_2(sq)_2]^+$ configuration is confirmed by the electrochemical and spectroscopic data. The shifts in couple **II** as functions of pyridine or dioxolene substituent (Figure 3) suggest that the redox process involves a largely dioxolene orbital, i.e. the b_{1u} LUMO. The PES $Ru(3d_{5/2})$ binding energies for those **O1** complexes measured lie on the boundary between normal Ru^{II} and Ru^{III},[31-38] and are higher than those of the **S** and **R1** complexes. Moreover, the FTIR spectra are typical of coordinated semiquinones, having no clearly identifiable ν(C-O), neither around 1650 (q) or 1250 cm^{-1} (cat)[26-30] nor at 1150 cm^{-1} as in **S**. The strongest bands in the spectra are pyridine vibrations around 1600 cm^{-1}, in some species, and the bands around 1450 cm^{-1}, where ν(C-O) and a number of other vibrations are expected.

All the **O1** species show one unpaired electron as indicated by magnetism or ESR studies. Frozen solutions of most **O1** complexes give asymmetric ESR signals with only one g value resolved, this being close to the free radical value of 2. However, two g values are resolved for all complexes in the solid state and two in frozen solution. The degree of anisotropy is small, similar

to that observed in $[Ru(bpy)_2(sq)]^+$, $[Ru(bpy)(diox)_2]^+$ and a range of ligand-centered radical complexes of the $[Ru(bpy)_2]^{2+}$ fragment.[6,9,57-59] While other solid state effects cannot be neglected, it is likely that exchange narrowing allows the resolution of the two intrinsic g values which cause the asymmetry of the other signals. Splitting of this type, $g_\perp < g_\parallel$, has previously been taken as an indication of some Ru^{III} contribution to the electronic ground state of Ru^{II}-semiquinone complexes.[6,9]

Using the MO picture in Figure 5, the Ru^{III} configuration results from strong mixing of the metal and ligand b_{2g} orbitals to give b_{2g} and $2b_{2g}^*$ MO's which each have about 50% metal character. The coupling is then to both equivalent semiquinone ligands leaving one unpaired electron distributed, in the b_{1u} orbital, over both semiquinones. The anisotropy seen in the ESR spectra then comes from mixing of a higher excited state which has the unpaired electron on the metal center.

The electronic spectra are also consistent with this MO description. The intense low energy electronic transition, occurring between 700 and 830 nm, band (**O1,I,II**) (Figure 4, Table VIII) is composite, being a strong band with a lower energy shoulder or peak. The higher energy component, band (**O1,II**), behaves very much like band (**S,I**) but with small dependences on both pyridine and dioxolene substituents (Figure 6). The substituent effects are in accord with assignment, as for (**S,I**), to the transition b_{1u} ---> $2b_{2g}^*$ which is intraligand with some LMCT character. It is broader than band (**S,I**) because the acceptor orbital has more anti-bonding character. For DTBDiox species:

Band (**O1,II**) $\nu(cm^{-1}) = -735\ E(Ru^{III/II}) + 12800$ (R = 0.80, 12 pts.)

(4)

The lower energy component (**O1,I**) also shifts to a small degree with pyridine substituent, in the opposite direction to band (**O1,II**), and falls under band (**O1,II**), for pyridines with electron-withdrawing substituents. Since band (**O1,I**) usually appears as a shoulder it gives a very scattered correlation when plotted against the $Ru^{III/II}$ potential. It moves to the red and becomes a clear

peak with less basic dioxolenes such as ClDiox (Table VIII). These observations lead to a Ru(dπ) ---> R'Diox MLCT assignment. There are two possible transitions which are expected to be relatively strong, namely Ru(b_{2g},b_{3g}) ---> R'Diox(b_{1u}). Since there appear no other reasonable candidates for these transitions in the visible region, they may both fall under the Band (**O1,I,II**) envelope.

At higher energies two weaker absorptions are observed, at 520 and 450 nm (bands (**O1,III,IV**)). These transitions have no clear correlation with pyridine substituent, but the peak near 450 nm shifts to the blue with less electron-donating dioxolenes. Two dioxolene n ---> π^* transitions, a_g ---> b_{1u} and b_{3u} ---> $2b_{2g}^*$, are allowed in **O1**. These are analogous to band (S,II) and are assigned to bands (**O1,III,IV**). Band (**O1,V**) at 380 nm can be assigned as the internal semiquinone π ---> π^* transition[55] since MLCT transitions involving the pyridine will be in the UV region and no low energy LMCT from pyridine is expected.

O2 Species. Owing to general species instability, no detailed spectroscopic analyses were undertaken; upon oxidation from **O1**, isosbestic points were usually poor or not present. However oxidation of **O1** Ru(3-ClPy)$_2$(DTBDiox)$_2$ and Ru(4-AcPy)$_2$(DTBDiox)$_2$ gave reasonable isosbestic points. The **O2** species produced had broad strong bands around 650 nm in DCE.

Table IX summarizes the assignments of transitions observed in the **R1**, **S** and **O1** species.

Concluding Remarks

In summary the trans-Ru(RPy)$_2$(R'Diox)$_2$ redox series are best represented as shown in Chart III.

Chart III

R2 $[Ru^{II}(RPy)_2(cat)_2]^{2-}$

R1 $[Ru^{III}(RPy)_2(cat)_2]^{-}$

S $Ru^{III}(RPy)_2(cat)(sq) <===> Ru^{II}(RPy)_2(sq)_2$

O1 $[Ru^{III}(RPy)_2(sq)_2]^{+}$

These conclusions differ slightly from the conclusions reached for the corresponding cis-bpy complexes shown in Chart II. Yet, on the basis of similarities in the FTIR and PES spectra, and Ru-O and dioxolene bond lengths in the S complexes, $Ru(bpy)_2(Diox)_2$ and $Ru(4\text{-}BuPy)_2(DTBDiox)_2$, the net electron transfer from the two dioxolenes to the metal (and therefore the degree of metal-ligand orbital mixing) is probably approximately equal in the cis and trans S species.

The real differences between the two series are due to symmetry affecting the distribution of metal and ligand electron density between orbitals. This results in electronic spectroscopic differences which have caused us to reach different conclusions regarding the "best representation" of the electronic structures of the two series.

In the trans species only one of the Ru "t_{2g}" orbitals can mix with the dioxolene π $3b_1$ orbital, whereas in the cis complexes all three t_{2g} orbitals are allowed by symmetry and overlap to mix with the dioxolene $3b_1$ set. Thus in the trans species two metal valence orbitals are non-bonding with respect to the dioxolene, and the b_{1u} level is pure ligand in nature (barring some mixing with metal $p\pi$).

Supposing that, in the S complexes, the valence metal and dioxolene ligand b_{2g} orbitals in the trans species mix to give two orbitals (b_{2g} and $2b_{2g}^*$) each of which is approximately 50% metal and 50% ligand character, the "oxidation state" of the metal approximates to Ru^{III} on the basis of the weighted populations of the valence orbitals. The lowest energy electronic transition (b_{1u} ---> $2b_{2g}^*$) then has LMCT character.

In the cis complexes all three metal levels mix with dioxolene π levels. The amounts of mixing will differ for the three orbitals, but if we assume the same net transfer of ligand electron density to the metal as in the trans series above, but now distributed over three d orbitals, we obtain approximate average populations of 70% d + 30% diox for the three "d" orbitals, and 55% diox + 45% d for the ligand π^* orbitals. This again gives an "oxidation state" of approximately Ru^{III} (5.1 valence electrons localized on the metal). However, in this case the lowest energy

electronic transition has MLCT (Ru ---> diox) character, as observed.

Our conclusions relating to the cis complexes were largely influenced by the electronic spectroscopic data for which a Ru^{II} description was most useful (particularly in view of the resonance Raman data showing a Ru ---> bpy CT transition), although we recognised that the real situation was not clearcut and that a MO picture was needed. Clearly for the trans species the Ru^{II} description is less useful, since transitions of LMCT character are seen. In the **O1** species the overall degree of metal-ligand mixing may also be similar in the cis and trans species but there is less evidence available to support this supposition. If this is so, then similar arguments apply.

It is also noteworthy that both the **S** and **O1** species are apparently best described as Ru^{III} species without the normal $4d^5$ configuration, **S** being diamagnetic and **O1** having a hole on the ligand.

There are clearly subtle new features arising from the study of redox series involving non-innocent, or redox active, ligands. The variation in ligand substitution in the pyridine series does not have a great influence on the electronic structure of each redox product but is extremely useful in assigning the electronic spectra of these species. Similar work has been completed on phosphine substituted species which offer a wider range of variation in the σ and π properties of the co-ligands,[60,61] and on the substitution of the oxygen atoms of the dioxolene ligands by nitrogen.[62]

Acknowledgments. We are indebted to the Natural Sciences and Engineering Research Council (Ottawa) and the Office of Naval Research (Washington) for financial support. We also thank Yu Hong Tse for recording some spectroscopic data, Dr. Lawrence Thompson (Memorial University) for magnetic measurements, and the Johnson Matthey Company for the loan of ruthenium trichloride.

References

1. Current addresses: (a) Chevron Chemical Company, Kingwood, TX. (b) Department of Chemistry, Mie University, Japan. (c) Department of Chemistry, Yangzhou Teacher's College, Jiangsu, People's Republic of China. (d) Central Research Laboratories, Kanegafuchi Chemical Industry Co. Ltd., Kobe 652, Japan.
2. Pierpont, C. G.; Buchanan, R. M Coord. Chem. Rev. **1981**, 38, 45.
3. Kaim, W. Coord. Chem. Rev. **1987**, 43.
4. McCleverty, J. A. Prog. Inorg. Chem. **1968**, 10, 49.
5. Schrauzer, G. N. Acc. Chem. Res. **1969**, 2, 72.
6. Haga, M.; Dodsworth, E. S.; Lever, A. B. P. Inorg. Chem. **1986**, 25, 447.
7. Haga, M.; Dodsworth, E. S.; Lever, A. B. P.; Boone, S. R.; Pierpont, C. G. J. Am. Chem. Soc. **1986**, 108, 7413.
8. Stufkens, D. J.; Snoeck, Th. L.; Lever, A. B. P. Inorg. Chem. **1988**, 27, 953.
9. Lever, A. B. P.; Auburn, P. R.; Dodsworth, E. S.; Haga, M.; Liu, W.; Melnik, M.; Nevin, W. A. J. Am. Chem. Soc. **1988**, 110, 8076.
10. Haga, M.; Isobe, K.; Boone, S. R.; Pierpont, C. G. Inorg. Chem. **1990**, 29, 3795.
11. Bhattacharya, S.; Boone, S. R.; Fox, G. A.; Pierpont, C. G. J. Am. Chem. Soc. **1990**, 112, 1088.
12. Tse, Y.-H., Auburn, P. R.; Lever, A. B. P. to be submitted for publication.
13. Wen, T.; Thompson, L. K.; Lee, F. L.; Gabe, E. J. Inorg. Chem. **1988**, 27, 4190.
14. Gennett, T.; Milner, D. F.; Weaver, M. J. J. Phys. Chem. **1985**, 89, 2787.
15. Mitchell, R. W.; Spencer, A.; Wilkinson, G. J. Chem. Soc. Dalton Trans. **1973**, 846.
16. Boone, S. R.; Pierpont, C. G. Inorg. Chem. **1987**, 26, 1769.
17. Boone, S. R.; Pierpont, C. G. Polyhedron **1990**, 9, 2267.
18. Hammett, L. P. Physical Organic Chemistry. Reaction Rates. Equilibria and Mechanisms,2nd Edn.; McGraw Hill, New York, 1970.

19. Gordon, D. J.; Fenske, R. F. Inorg. Chem. **1982**, 21, 2907,2916

20. DeSimone, R. E. J. Am. Chem. Soc. **1973**, 95, 6238.

21. Sakaki, S.; Hagiwara, N.; Yanase, Y.; Ohyoshi, A. J. Phys. Chem. **1978**, 82, 1917.

22. Raynor, J. B.; Jeliazkowa, B. G. J. Chem. Soc. Dalton Trans. **1982**, 1185.

23. Hudson, A.; Kennedy, M. J. J. Chem. Soc. A **1969**, 1116.

24. Lahiri, G. K.; Bhattacharya, S.; Ghosh, B. K.; Chakravorty, A. Inorg. Chem. **1987**, 26, 4324.

25. Pell, S. D.; Salmonsen, R. B.; Abelleira, A.; Clark, M. J. Inorg. Chem. **1984**, 23, 385.

26. Wicklund, P. A.; Brown, D. G. Inorg. Chem. **1976**, 15, 396.

27. Brown, D. G.; Reinprecht, J. T.; Vogel, G. C. Inorg. Nucl. Chem. Lett. **1976**, 12, 399.

28. Brown, D. G.; Johnson, W. L. Z. Naturforsch. **1979**, 34b, 712.

29. Lynch, M. W.; Valentine, M.; Hendrickson, D. N. J. Am. Chem. Soc. **1982**, 104, 6982.

30. Hartmann, J. R.; Foxman, B. M.; Cooper, S. R. Inorg. Chem. **1984**, 23, 1381.

31. Weaver, T. R.; Meyer, T. J.; Adeyemi, S. A.; Brown, G. M.; Eckberg, R. P.; Hatfield, W. P.; Johnson, E. C.; Murray, R. W.; Untereker, D. J. Am. Chem. Soc. **1975**, 97, 3039.

32. Connor, J. A.; Meyer, T. J.; Sullivan, B. P. Inorg. Chem. **1979**, 18, 1388.

33. Feltham, R. D.; Brant, P. J. Am. Chem. Soc. **1982**, 104, 641.

34. Srivastava, S. App. Spec. Rev. **1986**, 22, 401.

35. Geselowitz, D. A.; Kutner, W.; Meyer, T. J. Inorg. Chem. **1986**, 25, 2015.

36. Brant, P.; Stephenson, T. A. Inorg. Chem. **1987**, 26, 22.

37. Shepherd, R. E.; Proctor, A.; Henderson, W. W.; Myser, T. K. Inorg. Chem. **1987**, 26, 2440.

38. Gassman, P. G.; Winter, C. H. J. Am. Chem. Soc. **1988**, 110, 6130.

39. Lever, A. B. P. Inorganic Electronic Spectroscopy, 2nd Edn.; Elsevier: Amsterdam, 1984.

40. Salama, S.; Stong, J. D.; Neilands, J. B.; Spiro, T. G. Biochem. **1978**, 17, 3781.

41. Bristow, S.; Enemark, J. H.; Garner, C. D.; Minelli, M.; Morris, G. A.; Ortega, R. B. Inorg. Chem. **1985**, 24, 4070.

42. Cox, D. D.; Benkovic, S. J.; Bloom, L. M.; Bradley, F. C.; Nelson, M. J.; Que, L. Jr.; Wallick,

D. E. J. Am. Chem. Soc. **1988**, 110, 2026.

43. Dodsworth, E. S.; Lever, A. B. P. Chem. Phys. Lett. **1986**, 124, 152.

44. Clark, R. J. H.; Stead, M. J. J. Chem. Soc. Dalton Trans. **1981**, 1760.

45. deLearie, L. A.; Haltiwanger, R. C.; Pierpont, C. G. Inorg. Chem. **1987**, 26, 817.

46. deLearie, L. A.; Haltiwanger, R. C.; Pierpont, C. G. J. Am. Chem. Soc., **1989**, 111, 4324.

47. Lever, A. B. P. Inorg. Chem. **1990**, 29, 1271.

48. Buchanan, R. M.; Kessel, S. L.; Downs, H. H.; Pierpont, C. G.; Hendrickson, D. N. J. Am. Chem. Soc. **1978**, 100, 7894.

49. Faure, R.; Duc, G.; Deloume, J.-P. Acta Crystallogr. **1986**, C42, 982.

50. Rillema, D. P.; Jones, D. S.; Levy, H. A. J. Chem. Soc. Chem. Comm. **1979**, 849.

51. Thompson, J. S.; Calabrese, J. C. Inorg. Chem. **1985**, 24, 3167.

52. Buchanan, R. M.; Claflin, J.; Pierpont, C. G. Inorg. Chem. **1983**, 22, 2552.

53. Buchanan, R. M.; Pierpont, C. G. J. Am. Chem. Soc. **1980**, 102, 4951.

54. Robin, M. B.; Day, P. Adv. Inorg. Chem. Radiochem. **1967**, 10, 248.

55. Dodsworth, E. S.; Lever, A. B. P. Chem. Phys. Lett. **1990**, 172, 151.

56. Stufkens, D. J.; Lever, A. B. P. work in progress.

57. Motten, A. G.; Hanck, K. W.; DeArmond, M. K. Chem. Phys. Lett. **1981**, 79, 541.

58. Morris, D. E.; Hanck, K. W.; DeArmond, M. K. J. Am. Chem. Soc. **1983**, 105, 3032.

59. Morris, D. E.; Hanck, K. W.; DeArmond, M. K. Inorg. Chem. **1985**, 24, 977.

60. Bhattacharya, S.; Pierpont, C. G. Inorg. Chem. **1991**, 30, 1511.

61. Auburn, P. R.; Lever, A. B. P. to be submitted for publication.

62. Masui, H.; Auburn, P. R.; Lever, A. B. P. Inorg. Chem. **1991**, 30, 0000.

Table I. ^1H NMR Spectra of t-Ru(R-Py)$_2$(R′-Diox)$_2$, S, Complexes[a]

Complex	Chemical Shift, δ
Ru(3-AcPy)$_2$(DTBDiox)$_2$	8.03 (d, J=1.6 Hz, 2H); 7.83 (m, 2H); 7.71 (d, 2.1 Hz, 2H); 7.68 (dd, J=5.6, 1.4 Hz, 2H); 7.00 (dd, J=7.9, 5.7 Hz, 2H); 6.20 (d, J=2.1 Hz, 2H); 2.34 (s, 6H); 1.65 (s, 18H); 1.37 (s, 18H).
Ru(4-AcPy)$_2$(DTBDiox)$_2$	7.84 (d, J=6.9 Hz, 2H); 7.62 (d, J=2.1 Hz, 4H); 7.28 (dd, J=6.8, 1.5 Hz, 4H); 6.27 (br s, 2H); 2.40 (s, 6H); 1.64 (s, 18H); 1.36 (s, 18H).
Ru(3-ClPy)$_2$(DTBDiox)$_2$	7.74 (d, J=2.2 Hz, 2H); 7.63 (d, J=2.0 Hz, 2H); 7.60 (dd, J=5.4, 1.1 Hz, 2H); 7.23 (m, 2H); 6.87 (dd, J=8.2, 5.7 Hz, 2H); 6.17 (br s, 2H); 1.62 (s, 18H); 1.35 (s, 18H).
Ru(4-ClPy)$_2$(DTBDiox)$_2$	7.66 (d, J=2.1 Hz, 2H); 7.51 (dd, 5.4, 1.3 Hz, 4H); 6.84 (dd, J=5.4, 1.3 Hz, 4H); 6.13 (d, 1.9 Hz, 2H); 1.64 (s, 18H); 1.38 (s, 18H).
Ru(3-PhPy)$_2$(DTBDiox)$_2$	7.79 (d, J=2.1 Hz, 2H); 7.67 (d, J=1.9 Hz, 2H); 7.40 (m, 2H); 7.31 (m, 2H); 7.26 (m, 10H); 6.87 (m, 2H); 6.09 (d, J=2.1 Hz, 2H); 1.63 (s, 18H); 1.40 (s, 18H).
Ru(Py)$_2$(DTBDiox)$_2$	7.64 (s, 2H); 7.51 (d, J=5.1 Hz, 4H); 7.22 (t, J=7.5 Hz, 2H); 6 .79 (dd, J=7.5, 5.1 Hz, 4H); 5.92 (br s, 2H); 1.61 (s, 18H); 1.40 (s, 18H).
Ru(4-PhPy)$_2$(DTBDiox)$_2$	7.70 (d, J=2.2, 2H); 7.50 (d, J=6.9 Hz, 4H); 7.35 (br s, 10H); 7.02 (d, 6.6 Hz, 4H); 6.02 (d, J=2.2 Hz, 2H); 1.68 (s, 18H); 1.41 (s, 18H).
Ru(4-VPy)$_2$(DTBDiox)$_2$	7.75 (br s, 2H); 7.40 (d, J=6.1 Hz, 4H); 6.77 (d, J=6.1 Hz, 4H); 6.36 (dd, J=17.5, 10.8 Hz, 2H); 5.96 (br s, 2H); 5.70 (d, J=17.5, 2H); 5.34 (d, J=10.8 Hz, 2H); 1.66 (s, 18H); 1.48 (s, 18H).

Ru(4-MePy)$_2$(DTBDiox)$_2$ 7.78 (d, J=2.1 Hz, 2H); 7.20 (d, J=6.6 Hz, 4H); 6.59 (d, J=5.9 Hz, 4H); 5.95 (d, J=1.9 Hz, 2H); 2.17 (s, 6H); 1.65 (s, 18H); 1.42 (s, 18H).

Ru(3-EtPy)$_2$(DTBDiox)$_2$ 7.77 (br s, 2H); 7.27 (s, 2H); 7.20 (d, J=5.4 Hz, 2H); 7.00 (d, J=7.7 Hz, 2H); 6.68 (dd, J=7.7, 5.6 Hz, 2H); 5.98 (br s, 2H); 2.22 (q, J=7.6 Hz, 4H); 1.65 (s, 18H); 1.40 (s, 18H); 0.93 (t, J=7.6 Hz, 6H).

Ru(4-EtPy)$_2$(DTBDiox)$_2$ 7.78 (d, J=2.1 Hz, 2H); 7.21 (d, J=6.6 Hz, 4H); 6.60 (d, J=6.6 Hz, 4H); 5.94 (br s, 2H); 2.45 (q, J=7.6 Hz, 4H); 1.66 (s, 18H); 1.42 (s, 18H); 0.99 (t, J=7.6 Hz, 6H).

Ru(4-BuPy)$_2$(DTBDiox)$_2$ 8.33 (d, J=2.1 Hz, 2H); 7.37 (d, J=6.6 Hz, 4H); 6.15 (d, J=2.1 Hz, 2H); 6.09 (d, J=6.6 Hz, 4H); 2.03 (s, 18H); 1.44 (s, 18H); 0.39 (s, 18H).

Ru(3-ClPy)$_2$(TBDiox)$_2$ 7.64 (d, J=2.1 Hz, 2H); 7.53 (d, 2.2 Hz, 2H); 7.50 (d, J=8.8 Hz, 2H); 7.43 (dd, J=5.6, 1.0 Hz, 2H); 6.80 (d, J=5.7 Hz, 2H); 6.78 (d, J=5.9 Hz, 2H); 6.27 (dd, J=8.8, 2.2 Hz, 1.5H); 6.18 (dd, J=8.8, 2.2 Hz, 0.5H): 1.38 (s, 18H).

Ru(4-PhPy)$_2$(TBDiox)$_2$ 7.75 (m, 2H); 7.60 (m, 2H); 7.34-7.26 (m, 14H); 7.04 (m, 4H); 6.09 (dd, J=8.7, 2.1, 1.2H); 5.99 (dd, J=8.7, 2.1 Hz, 0.8H); 1.44 (s, 18H).

Ru(4-VPy)$_2$(TBDiox)$_2$ 7.72 (m, 2H); 7.52 (m, 2H); 7.16 (m, 4H); 6.78 (m, 4H); 6.37 (dd, J=17.6, 10.8 Hz, 2H); 6.05 (dd, J=8.7, 2.2 Hz, 1H); 5.95 (dd, J=8.7, 2.2 Hz, 1H); 5.65 (d, 17.6 Hz, 2H); 5.31 (d, J=10.8 Hz, 2H); 1.45 (s, 18H).

---

a) Obtained at 300 mHz in $CDCl_3$ solution. The chemical shifts are reported in parts per million (δ) downfield from tetramethylsilane. s = singlet, d = doublet, t = triplet, q = quartet, m = multiplet.

Table II. ESR Data for [Cp_2Co][t-[$Ru(R\text{-}Py)_2(R'\text{-}Diox)_2$]][a], R1

	g_1	g_2[b]	g_3
[Cp_2Co][$Ru(3\text{-}AcPy)_2(DTBDiox)_2$]	2.32	2.12(176)	(c)
[Cp_2Co][$Ru(4\text{-}AcPy)_2(DTBDiox)_2$]	2.34	2.11(175)	1.91
[Cp_2Co][$Ru(3\text{-}ClPy)_2(DTBDiox)_2$]	2.31	2.15(69)	1.82
[Cp_2Co][$Ru(3\text{-}ClPy)_2(DTBDiox)_2$][d]	2.30	2.15	1.80
[Cp_2Co][$Ru(4\text{-}ClPy)_2(DTBDiox)_2$]	2.31	2.15(100)	1.82
[Cp_2Co][$Ru(3\text{-}PhPy)_2(DTBDiox)_2$]	2.36	2.15(94)	2.01
[Cp_2Co][$Ru(Py)_2(DTBDiox)_2$]	2.35	2.16(103)	1.82
[Cp_2Co][$Ru(4\text{-}PhPy)_2(DTBDiox)_2$]	2.34	2.16(84)	1.81
[Cp_2Co][$Ru(4\text{-}VPy)_2(DTBDiox)_2$]	2.35	2.16(85)	1.86
[Cp_2Co][$Ru(4\text{-}MePy)_2(DTBDiox)_2$]	2.22	2.16(120)	1.87
[Cp_2Co][$Ru(3\text{-}EtPy)_2(DTBDiox)_2$]	2.34	2.16(98)	1.78
[Cp_2Co][$Ru(4\text{-}EtPy)_2(DTBDiox)_2$]	2.34	2.18(130)	1.77
[Cp_2Co][$Ru(4\text{-}BuPy)_2(DTBDiox)_2$]	2.30	2.18(110)	1.77
[Cp_2Co][$Ru(3\text{-}ClPy)_2(TBDiox)_2$]	2.36	2.17(117)	1.80
[Cp_2Co][$Ru(4\text{-}PhPy)_2(TBDiox)_2$]	2.35	2.18(74)	(c)
[Cp_2Co][$Ru(4\text{-}VPy)_2(TBDiox)_2$]	2.36	2.18(70)	(c)

a) Samples were prepared <u>in situ</u> by addition of a solution of Cp_2Co in DCE to the solid starting material. Spectra were recorded at 110-115K. b) Peak-peak separation in parentheses. c) Due to broadness g_3 is undefined. d) Solid state data at 77 K.

Table III. ESR Data for *t*-[Ru(R-Py)$_2$(R'-Diox)$_2$]$^+$, **O1**, Salts

	Frozen solution[a,b]		Solid state[a]	
	$g_\perp$	$g_\parallel$	$g_\perp$	$g_\parallel$
[Ru(3-AcPy)$_2$(DTBDiox)$_2$]PF$_6$	2.01[d](130)		1.98[d](84)	2.09
[Ru(4-AcPy)$_2$(DTBDiox)$_2$]PF$_6$	2.00[d](115)		1.98[d](74)	2.10
[Ru(3-ClPy)$_2$(DTBDiox)$_2$]ClO$_4$	2.00[c](110)		1.99[d](88)	2.07
[Ru(3-ClPy)$_2$(DTBDiox)$_2$]SO$_3$CF$_3$	2.01[c](87)		1.99[c](50)	2.07
[Ru(4-ClPy)$_2$(DTBDiox)$_2$]PF$_6$	2.00[d](157)		1.99[d](145)	2.10
[Ru(3-PhPy)$_2$(DTBDiox)$_2$]PF$_6$	2.01[d](153)		1.98[d](104)	2.10
[Ru(Py)$_2$(DTBDiox)$_2$]PF$_6$	1.99[d](166)		1.97[d](100)	2.07
[Ru(4-PhPy)$_2$(DTBDiox)$_2$]SO$_3$CF$_3$	1.98[d](123)	2.14	1.97[c](53)	2.12
[Ru(4-VPy)$_2$(DTBDiox)$_2$]PF$_6$	1.99[d](122)	2.09	1.98[d](95)	2.08
[Ru(4-MePy)$_2$(DTBDiox)$_2$]ClO$_4$	2.01[d](190)		1.97[c](53)	2.10
[Ru(4-MePy)$_2$(DTBDiox)$_2$]SO$_3$CF$_3$	2.01[c](140)		1.96[c](43)	2.16
[Ru(3-EtPy)$_2$(DTBDiox)$_2$]PF$_6$	2.01[d](150)		1.99[d](92)	2.10
[Ru(4-EtPy)$_2$(DTBDiox)$_2$]PF$_6$	2.01[d](147)		1.99[d](108)	2.08
[Ru(4-BuPy)$_2$(DTBDiox)$_2$]SO$_3$CF$_3$	2.00[c](135)		1.98[c](35)	2.03
[Ru(3-ClPy)$_2$(TBDiox)$_2$]PF$_6$	2.01[c](120)		1.99[c](115)	2.10
[Ru(4-PhPy)$_2$(TBDiox)$_2$]PF$_6$	2.01[d](210)		1.98[d](120)	2.17
[Ru(4-VPy)$_2$(TBDiox)$_2$]PF$_6$	2.01[d](208)		2.01[d](290)	

a) A single value is an unresolved signal probably closely associated with $g_\perp$. b) Solvent DCE. c) 77 K. d) 115 K. Peak-peak separations in parentheses.

Table IV. Electrochemical Data for t-Ru(R-Py)$_2$(R′-Diox)$_2$ Complexes[a]

Complex	$E_{1/2}$ vs SCE				
	I[b]	II	III	IV	
	O2	O1	S	R1	R2
Ru(3-AcPy)$_2$(DTBDiox)$_2$	+1.11	+0.32	-0.57	-1.50qr	
Ru(4-AcPy)$_2$(DTBDiox)$_2$	+1.08	+0.34	-0.55	-1.27qr	
Ru(3-ClPy)$_2$(DTBDiox)$_2$	+1.08	+0.30	-0.60	-1.51qr	
Ru(4-ClPy)$_2$(DTBDiox)$_2$	+1.11	+0.29	-0.62	-1.59ir	
Ru(3-PhPy)$_2$(DTBDiox)$_2$	+1.11	+0.26	-0.63	-1.63ir	
Ru(Py)$_2$(DTBDiox)$_2$	+1.07	+0.25	-0.65	-1.63ir	
Ru(4-PhPy)$_2$(DTBDiox)$_2$	+1.07	+0.24	-0.66	-1.56ir	
Ru(4-VPy)$_2$(DTBDiox)$_2$	+1.07	+0.24	-0.66	-1.55qr	
Ru(4-MePy)$_2$(DTBDiox)$_2$	+1.05	+0.24	-0.67	-1.72ir	
Ru(3-EtPy)$_2$(DTBDiox)$_2$	+1.08	+0.23	-0.68	-1.69ir	
Ru(4-EtPy)$_2$(DTBDiox)$_2$	+1.06	+0.23	-0.68	-1.71ir	
Ru(4-BuPy)$_2$(DTBDiox)$_2$	+1.07	+0.23	-0.68	-1.70ir	
Ru(3-ClPy)$_2$(TBDiox)$_2$	+1.20	+0.41	-0.41	-1.34qr	
Ru(4-PhPy)$_2$(TBDiox)$_2$	+1.14	+0.34	-0.50	-1.47qr	
Ru(4-VPy)$_2$(TBDiox)$_2$	+1.15	+0.35	-0.51	-1.46	
Ru(4-BuPy)$_2$(TBDiox)$_2$	+1.12	+0.36	-0.50	-1.56ir	
Ru(4-BuPy)$_2$(MeDiox)$_2$	+1.12	+0.36	-0.49	-1.55ir	
Ru(4-BuPy)$_2$(Diox)$_2$	+1.25	+0.44	-0.45	-1.57qr	
Ru(4-BuPy)$_2$(ClDiox)$_2$	+1.35	+0.61	-0.28	-1.44qr	

a) Measurements were made using 1,2 dichloroethane solutions of the starting materials (~10^{-3} M) containing ~0.2 M TBAP or TBAH. $E_{1/2}$

values are obtained from cyclic voltammetry at 100 mVs^{-1}. b) DTBDiox complexes showed a third oxidation process with E_{pa} between +1.7 and +2.0 V, appearing as a shoulder close to the solvent limit and having no cathodic peak. qr = quasi-reversible, ir = irreversible.

Table V. Photoelectron Emission Data[a]

Complex	Ru(3d5/2)	O(1s)[b]	N(1s)[b]
R1:			
$[Cp_2Co][Ru(3\text{-}ClPy)_2(DTBDiox)_2]$	281.4[c]	528.2(0.22)	399.2(0.83)
		529.9(0.56)	397.7(0.17)
		531.3(0.22)	
S:			
$Ru(3\text{-}ClPy)_2(DTBDiox)_2$	280.8	530.8(0.47)	400.3(0.76)
		532.2(0.33)	401.3(0.24)
		533.5(0.20)	
$Ru(Py)_2(DTBDiox)_2$	281.0	d	400.4(0.79)
			399.6(0.21)
$Ru(4\text{-}BuPy)_2(DTBDiox)_2$	280.9	d	400.3(0.71)
			399.3(0.29)
O1:			
$[Ru(3\text{-}ClPy)_2(DTBDiox)_2]ClO_4$	281.8	d	400.5
$[Ru(4\text{-}MePy)_2(DTBDiox)_2]ClO_4$	281.9	530.6(0.27)	399.3(1.0)
		531.8(0.45)	
		533.1(0.24)	
		534.3(0.04)	

a) Standardized to C(1s) at 285 eV. Errors vary between runs from ±0.1 to ±0.3 eV. b) Relative intensities of Gaussian components in parentheses. c) Average of two runs; data may be suspect due to charging problems. d) Contaminated with silicone grease.

Table VI. Electronic Spectroscopic Data for t-[Ru(R-Py)$_2$(R'-Diox)$_2$]$^-$, **R1**, Complexes

Complex	λ_{max}/nm (approx. log ϵ)[a]				
	(**R1**,I)	(**R1**,II)	(**R1**,III)	(**R1**,IV)	Conditions
[Ru(3-AcPy)$_2$(DTBDiox)$_2$]$^-$	840(3.85)	br	450(3.67)	372	TBAH/DCE
	845	br	450sh		Cp_2Co/DCE
[Ru(3-ClPy)$_2$(DTBDiox)$_2$]$^-$	b	545(3.52)	457(3.56)	368	TBAH/DCE
	865	534	450		Cp_2Co/DCM
[Ru(4-ClPy)$_2$(DTBDiox)$_2$]$^-$	b	532(3.43)	444sh	365(3.81)	TBAP/DCE
	835				Cp_2Co/DCE
[Ru(3-PhPy)$_2$(DTBDiox)$_2$]$^-$	845(3.78)	520sh	450sh	360sh	TBAH/DCE
	820				Cp_2Co/DCE
[Ru(Py)$_2$(DTBDiox)$_2$]$^-$	825(3.85)	484sh	400(3.62)	350sh	TBAH/DCE
	814				Cp_2Co/DCE
[Ru(4-PhPy)$_2$(DTBDiox)$_2$]$^-$	b	587	465	375	TBAP/DCE
	836	574	480		Cp_2Co/DCE
[Ru(4-VPy)$_2$(DTBDiox)$_2$]$^-$	b	608(3.64)	486(3.62)	380(3.84)	TBAH/DCE
	845	620	492	380sh	Cp_2Co/DCE
[Ru(4-MePy)$_2$(DTBDiox)$_2$]$^-$	806(3.89)	476sh			Cp_2Co/DCE
[Ru(3-EtPy)$_2$(DTBDiox)$_2$]$^-$	830(3.80)	492(3.50)	398sh	354sh	TBAH/DCE
	811	495sh			Cp_2Co/DCE
[Ru(4-EtPy)$_2$(DTBDiox)$_2$]$^-$	b	494sh	397(3.65)		TBAP/DCE
	807(3.90)	476sh			Cp_2Co/DCE
[Ru(4-BuPy)$_2$(DTBDiox)$_2$]$^-$	804	497		303	TBAP/DCE
	804(3.82)	486sh			Cp_2Co/DCE
[Ru(3-ClPy)$_2$(TBDiox)$_2$]$^-$	850(3.81)	516sh	450(3.65)	360(3.70)	TBAH/DCE

$[Ru(4\text{-}PhPy)_2(TBDiox)_2]^-$	802(3.84)	540	500sh		Cp_2Co/DCE
$[Ru(4\text{-}VPy)_2(TBDiox)_2]^-$	804(3.81)	sh	488		Cp_2Co/DCE
$[Ru(4\text{-}BuPy)_2(Diox)_2]^-$	750	470sh	407	301	TBAP/DCE
$[Ru(4\text{-}BuPy)_2(ClDiox)_2]^-$	741	463sh	412	307	TBAP/DCE

a) Samples were prepared <u>in situ</u> by the addition of Cp_2Co to solutions of the corresponding starting materials, or by bulk electrolysis of the starting materials in DCE solutions which were approximately 0.5 M in TBAH or TBAP. Some differences in the low energy peak positions are observed for the same species generated by the two methods. This is probably due to ion-pairing effects. sh = shoulder.

Table VII. Electronic Spectroscopic Data for t-Ru(R-Py)$_2$(R'-Diox)$_2$, S, Complexes

Complex	λ_{max}/nm (approx. log ϵ)				
	(S,I)	(S,II)	(S,III)	(S,IV)	Solvent
Ru(3-AcPy)$_2$(DTBDiox)$_2$	1155(4.48) 1110sh	585(3.09)	395(3.69)	318sh[a]	DCB
Ru(3-ClPy)$_2$(DTBDiox)$_2$	1160(4.54) 1110sh	584(3.01)	400sh 371(3.71)	320sh[a]	DCB
Ru(4-ClPy)$_2$(DTBDiox)$_2$	1160 1110sh	576	406 [illegible]	318sh[a]	DCB
Ru(3-PhPy)$_2$(DTBDiox)$_2$	1153(4.51) 1110sh	580(3.07)	408(3.68) 360sh	320sh[a]	DCB
Ru(Py)$_2$(DTBDiox)$_2$	1155(4.47) 1100sh	580(3.05)	403(3.64)	324(3.84)	DCE
Ru(4-PhPy)$_2$(DTBDiox)$_2$	1160(4.56) 1110sh	576(3.10)	450sh 380(3.88)	320sh[a]	DCB
Ru(4-VPy)$_2$(DTBDiox)$_2$	1163(4.68) 1115sh	574(3.23)	450sh 397(3.87)	316[a]	DCB
Ru(4-MePy)$_2$(DTBDiox)$_2$	1160(4.56) 1105sh	575(3.06)	402(3.58)	326[a]	DCB
Ru(3-EtPy)$_2$(DTBDiox)$_2$	1165(4.59) 1110sh	574(3.06)	404(3.63)	325[a]	DCB
Ru(4-EtPy)$_2$(DTBDiox)$_2$	1160(4.58) 1110sh	572(3.10)	400(3.64)	323[a]	DCB
Ru(4-BuPy)$_2$(DTBDiox)$_2$	1160(4.55) 1110sh	577(3.04)	400(3.58)	324(3.61)	DCE

$Ru(3\text{-}ClPy)_2(TBDiox)_2$	1165(4.53)	575(3.04)	402(3.65)		DCB
	1115sh		372sh		
$Ru(4\text{-}PhPy)_2(TBDiox)_2$	1165(4.52)	582(3.05)	400sh	320sh	DCE
	1115sh		366sh		
$Ru(4\text{-}VPy)_2(TBDiox)_2$	1165(4.55)	576(3.04)	454sh		DCB
	1115sh		380(3.80)		
$Ru(4\text{-}BuPy)_2(TBDiox)_2$	1161(4.69)	567(3.04)	390(3.64)	323(3.98)	DCE
	1110(4.67)				
$Ru(4\text{-}BuPy)_2(MeDiox)_2$	1155(4.46)	562(2.90)	388sh	323(3.81)	DCE
	1102(4.43)				
$Ru(4\text{-}BuPy)_2(Diox)_2$	1132(4.47)	560(3.04)	386sh	315(4.0)	DCE
	1080(4.46)				
$Ru(4\text{-}BuPy)_2(ClDiox)_2$	1144(4.38)	563(2.98)	393sh	324sh	DCE
	1088sh				

---

a) Observed in DCE solution. sh = shoulder.

Table VIII. Electronic Spectroscopic Data for $[Ru(R\text{-}Py)_2(R'\text{-}Diox)_2]^+$, **O1**, Complexes

Complex	λ_{max}/nm (approx. log ϵ)					
	(O1,I)	**(O1,II)**	**(O1,III)**	**(O1,IV)**	**(O1,V)**	Solvent
$[Ru(3\text{-}AcPy)_2(DTBDiox)_2]^+$		721(4.29)	520sh	448(3.37)	382(3.68)	DCE
$[Ru(4\text{-}AcPy)_2(DTBDiox)_2]^+$		726(4.23)	532sh	450(3.42)	378	DCE
$[Ru(3\text{-}ClPy)_2(DTBDiox)_2]^+$		720(4.27)	530sh	450(3.36)	381(3.71)	DCE
$[Ru(4\text{-}ClPy)_2(DTBDiox)_2]^+$		721(4.20)	536sh	450(3.26)	374(3.60)	DCE
$[Ru(3\text{-}PhPy)_2(DTBDiox)_2]^+$	800sh	717(4.17)	520sh	448(3.28)	380(3.59)	DCE
$[Ru(Py)_2(DTBDiox)_2]^+$	805sh	716(4.26)	518sh	450(3.28)	380(3.57)	DCE
$[Ru(4\text{-}PhPy)_2(DTBDiox)_2]^+$	820sh	728(4.25)	530sh	450sh	372(3.78)	DCB
$[Ru(4\text{-}VPy)_2(DTBDiox)_2]^+$	816sh	720(4.12)	528sh	450(3.28)	380sh	DCE
$[Ru(4\text{-}MePy)_2(DTBDiox)_2]^+$	818sh	713(4.14)	530sh	450(3.29)	384(3.51)	DCE
$[Ru(3\text{-}EtPy)_2(DTBDiox)_2]^+$	800sh	710(4.24)	520sh	446(3.35)	380(3.58)	DCE
$[Ru(4\text{-}EtPy)_2(DTBDiox)_2]^+$	798sh	711(4.08)	520sh	448(3.21)	383(3.45)	DCE
$[Ru(4\text{-}BuPy)_2(DTBDiox)_2]^+$	810sh	710(4.19)	526sh	446(3.30)	383(3.54)	DCE
$[Ru(3\text{-}ClPy)_2(TBDiox)_2]^+$		722(4.12)	536sh	444(3.11)	368(3.48)	DCE
$[Ru(4\text{-}PhPy)_2(TBDiox)_2]^+$	800sh	712(4.04)		440sh	370sh	DCM
$[Ru(4\text{-}VPy)_2(TBDiox)_2]^+$	796sh	716(4.22)	528sh	438sh	366sh	DCE
$[Ru(4\text{-}BuPy)_2(Diox)_2]^+$	818	688	520sh	440	374	DCE
$[Ru(4\text{-}BuPy)_2(ClDiox)_2]^+$	828	703	520sh	436	385	DCE

In general, pectra recorded in DCB show a red shift of between 5 and 15 nm in the low energy bands, compared with DCE or DCM. sh = shoulder.

Table IX. Summary of Electronic Transition Assignments

R1:			
Band (R1,I)	b_{1u} ---> $2b_{2g}$*	cat(π) ---> Ru(dπ)	LMCT
Band (R1,II)	a_g ---> b_{3u}*	Ru(dπ) ---> RPy(π*)	MLCT
	b_{2g} ---> b_{3u}*	cat(π) ---> RPy(π*)?	LLCT
Band (R1,III)	$2b_{2g}$* ---> b_{3u}*	Ru(dπ) ---> RPy(π*)	MLCT
Band (R1,IV)		cat(π) ---> Ru(dπ)?	LMCT
	b_{1u} ---> $3b_{2g}$*	cat(π) ---> RPy(π*)?	LLCT
S:			
Band (S,I)	b_{1u} ---> $2b_{2g}$*	R'Diox(π*) ---> Ru(dπ)+R'Diox(π*)	LMCT/IL[a]
Band (S,II)	b_{3u} ---> $2b_{2g}$*	R'Diox(n) ---> Ru(dπ)+R'Diox(π*)	LMCT/IL
Band (S,III)	b_{2g},a_g ---> b_{3u}*	Ru(dπ) ---> RPy(π*)	MLCT
Band (S,IV)		R'Diox(π) ---> R'Diox(π*)	IL
O1:			
Band (O1,I)	b_{2g},b_{3g} ---> b_{1u}	Ru(dπ) ---> sq(π*)	MLCT
Band (O1,II)	b_{1u} ---> $2b_{2g}$*	sq(π*) ---> Ru(dπ)+sq(π*)	LMCT/IL
Band (O1,III)	a_g ---> b_{1u}	sq(n) ---> sq(π*)	IL
Band (O1,IV)	b_{3u} ---> $2b_{2g}$*	sq(n) ---> Ru(dπ)+sq(π*)	LMCT/IL
Band (O1,V)	sq(π) ---> b_{1u}	sq(π) ---> sq(π*)	IL

a) Intraligand. The * designation in column 2 refers to orbitals which are antibonding in the MO scheme for the complex (Figure 5). In column 3 the * refers to free ligand orbitals. The semiquinone π ($3b_1$ in the

free ligand) orbital which is a π level in catechol and π^* in quinone is regarded as π^* here in both S and O1.

Figure Legends

Figure 1.

ESR spectra of (left) **R1** $[Cp_2Co][Ru(3\text{-}ClPy)_2(DTBDiox)_2]$, and (right) $[Ru(4\text{-}MePy)_2(DTBDiox)_2]ClO_4$, both in the solid state at 77 K. The arrows denote the postions of the DPPH signals.

Figure 2.

Cyclic voltammogram of 8.5×10^{-4} M $Ru(4\text{-}ClPy)_2(DTBDiox)_2$ in DCE solution containing 0.2 M TBAH. Scan rate 100 mV s^{-1}.

Figure 3.

Variation of the redox potentials of (a) $Ru(RPy)_2(DTBDiox)_2$ complexes with the Hammett σ parameters for the pyridine substituents (slopes: I, 0.02; II, 0.08; III, 0.09; IV, 0.24), and (b) $Ru(4\text{-}BuPy)_2(R'Diox)_2$ complexes with the Hammett σ parameters for the dioxolene substituents (slopes: I, 0.25; II, 0.31; III, 0.31; IV, 0.19). The Hammett parameters are multiplied by the number of substituents in the complex. For the 4-R'Diox complexes the para and meta parameters are averaged to account for the substituent effect at both oxygens. For DTBDiox the average of the para and meta σ values is doubled to account for both t-butyl groups, assuming the substituent effects for the ortho and para positions are equal.

Figure 4.

Visible-NIR spectra in DCE solution of (top) **R1** $[Ru(3\text{-}ClPy)_2(TBDiox)_2]^-$ generated electrochemically, (middle) **S** $Ru(Py)_2(DTBDiox)_2$, and (bottom) **O1** $[Ru(3\text{-}AcPy)_2(DTBDiox)_2]PF_6$ (——) and $[Ru(3\text{-}EtPy)_2(DTBDiox)_2]PF_6$ (---). The discontinuity around 850 nm in the S spectrum is an

instrumental artefact.

Figure 5.

Qualitative molecular orbital diagrams for (left) **R1**, and (right) **S** and **O1** species. These are based on group theory (D_{2h} symmetry) and the electronic spectra and are not to scale. The ordering of the MO's is probably the same for **S** and **O1** though the relative energies and amount of mixing will differ somewhat. The singly occupied HOMO's in **R1** and **O1** are denoted by arrows. The **O1** HOMO is doubly occupied in **S**. Ligand orbital symmetries are those given by Fenske.[18] The free ligand lone pair orbitals ($9a_1$) are indicated but for simplicity they are not included in the MO's of the complex.

Figure 6.

Plots showing the variation of selected charge transfer bands with the $Ru^{III/II}$ potential, couple **IV**, for DTBDiox complexes. The linear regressions do not include the data for the 4-vinyl- and 4-phenylpyridine complexes.

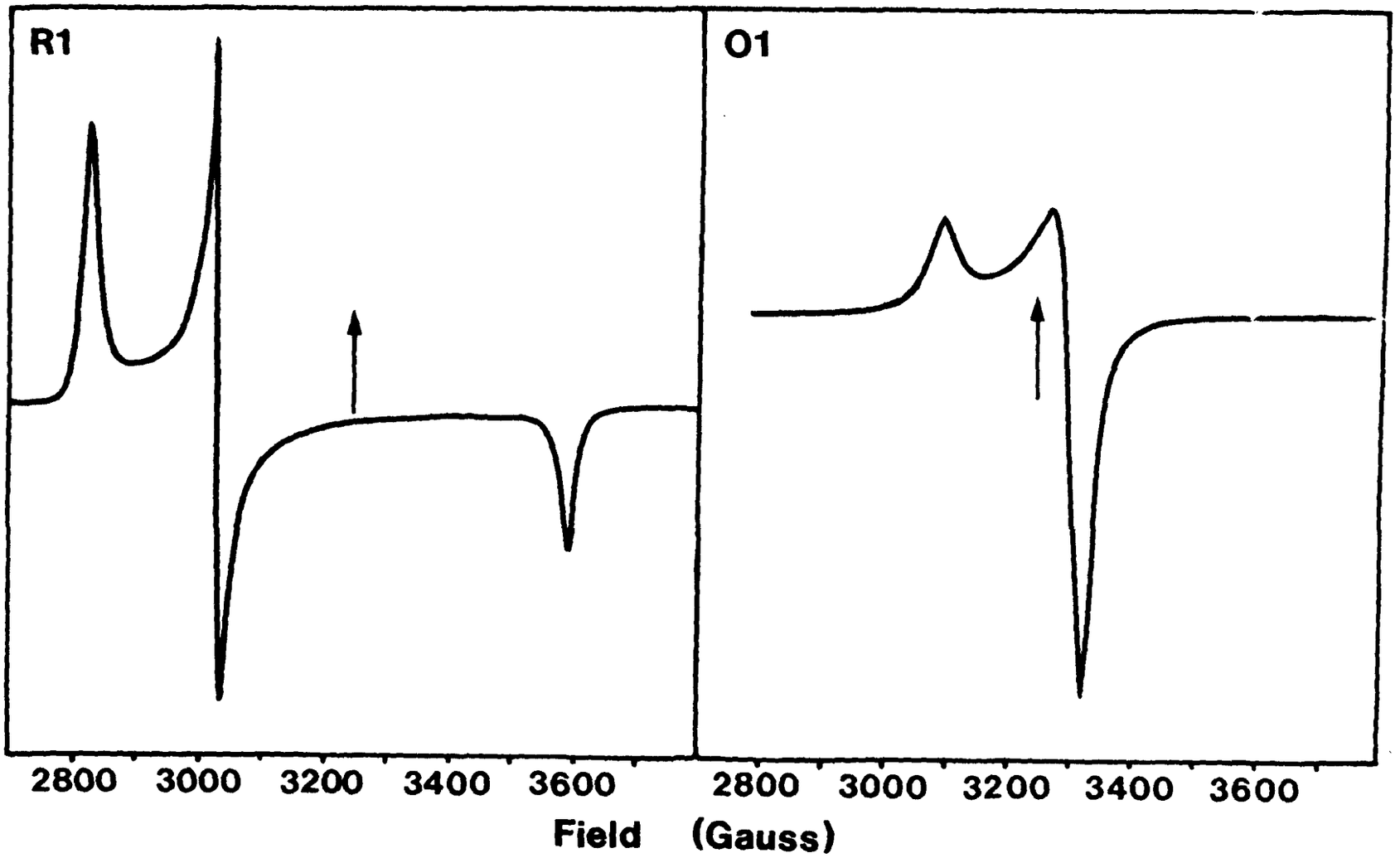
R1
O1
2800
3000
3200
3400
3600
2800
3000
3200
3400
3600
Field (Gauss)

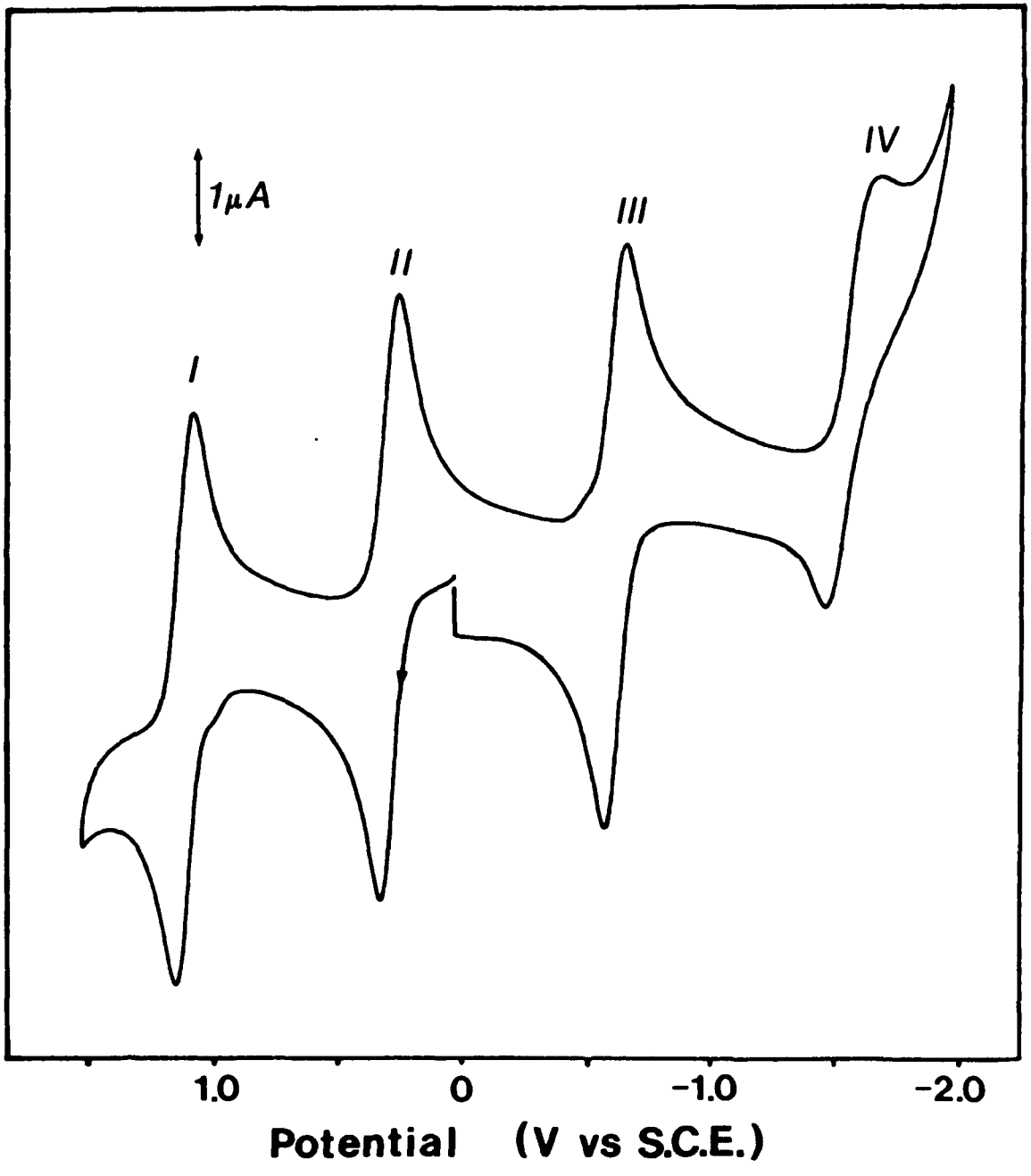
1μA
I
II
III
IV
1.0
0
-1.0
-2.0
Potential (V vs S.C.E.)

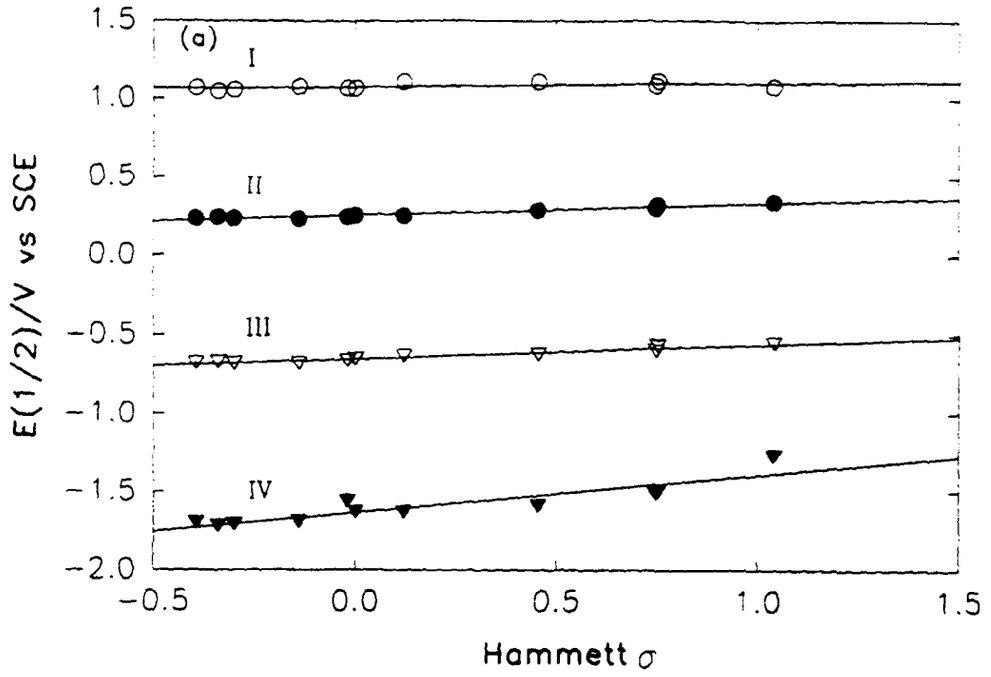
(a)
I
II
III
IV
E(1/2)/V vs SCE
Hammett σ
1.5
1.0
0.5
0.0
−0.5
−1.0
−1.5
−2.0
−0.5
0.0
0.5
1.0
1.5

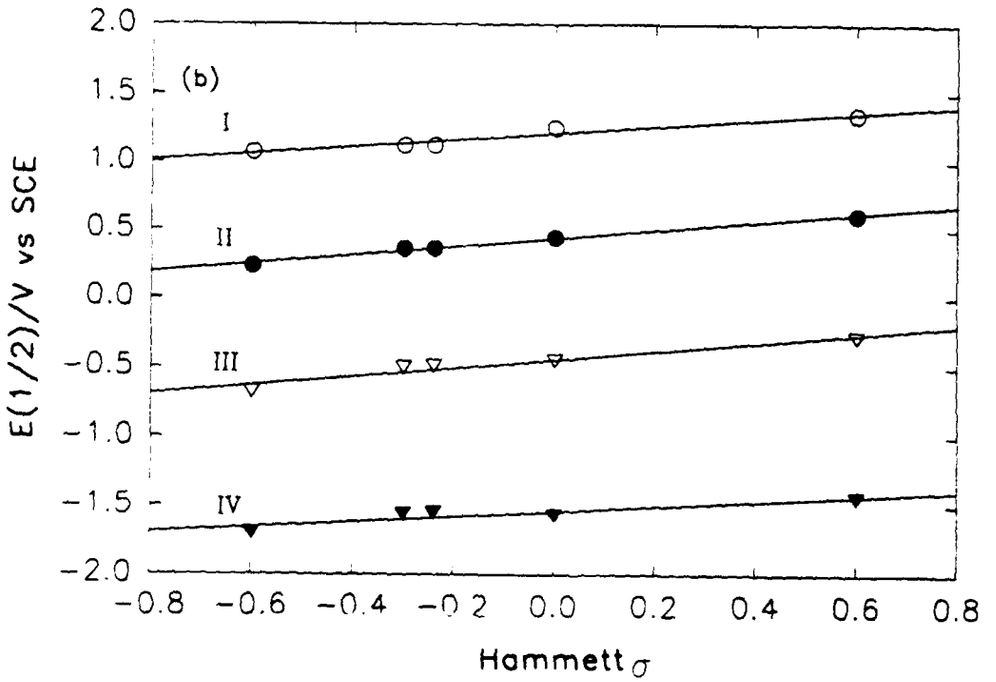
(b)
I
II
III
IV
E(1/2)/V vs SCE
Hammett σ
2.0
1.5
1.0
0.5
0.0
−0.5
−1.0
−1.5
−2.0
−0.8
−0.6
−0.4
−0.2
0.0
0.2
0.4
0.6
0.8

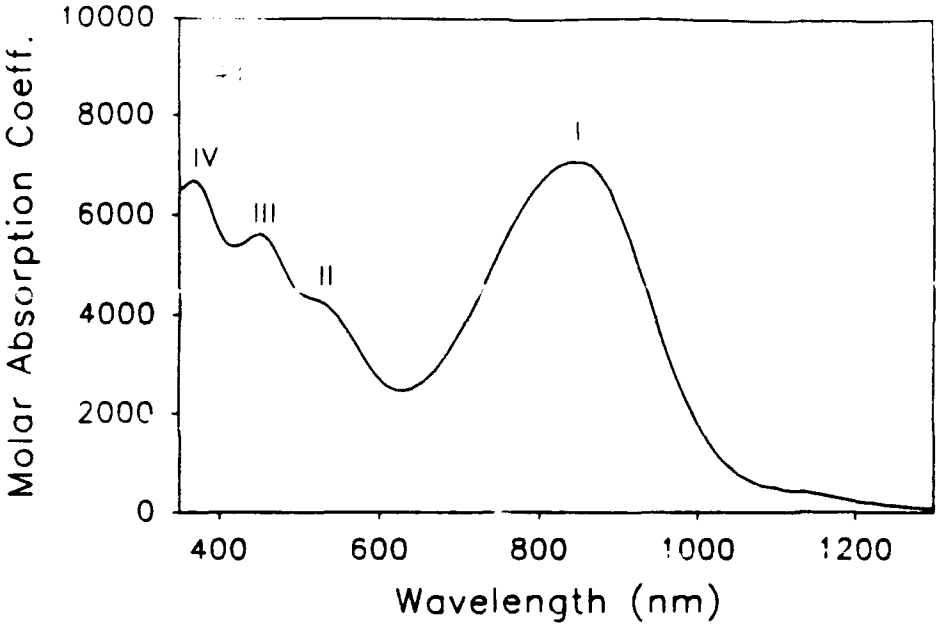
10000
8000
6000
4000
2000
0
Molar Absorption Coeff.
IV
III
II
I
400
600
800
1000
1200
Wavelength (nm)

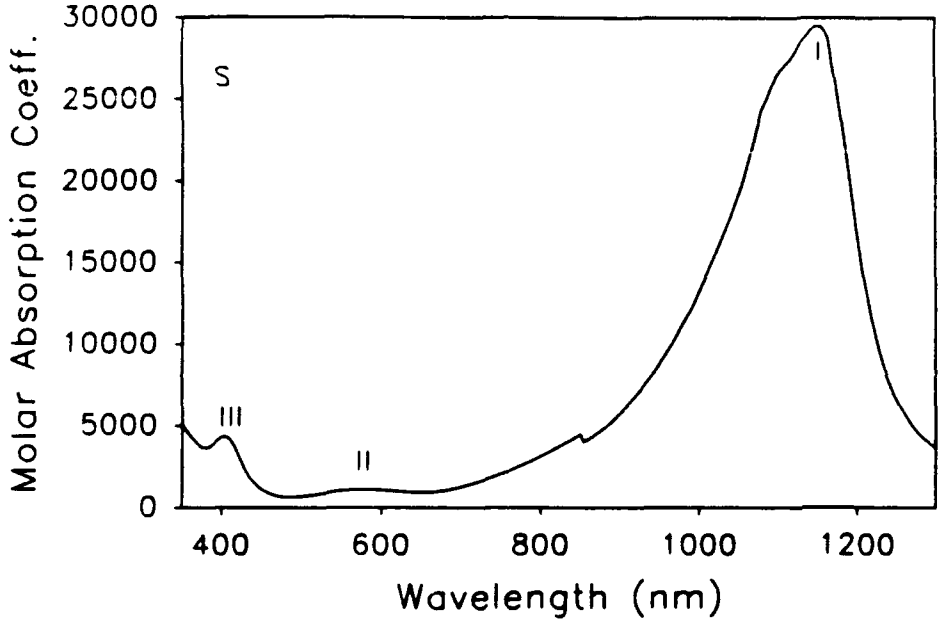
30000
25000
20000
15000
10000
5000
0
Molar Absorption Coeff.
S
III
II
I
400
600
800
1000
1200
Wavelength (nm)

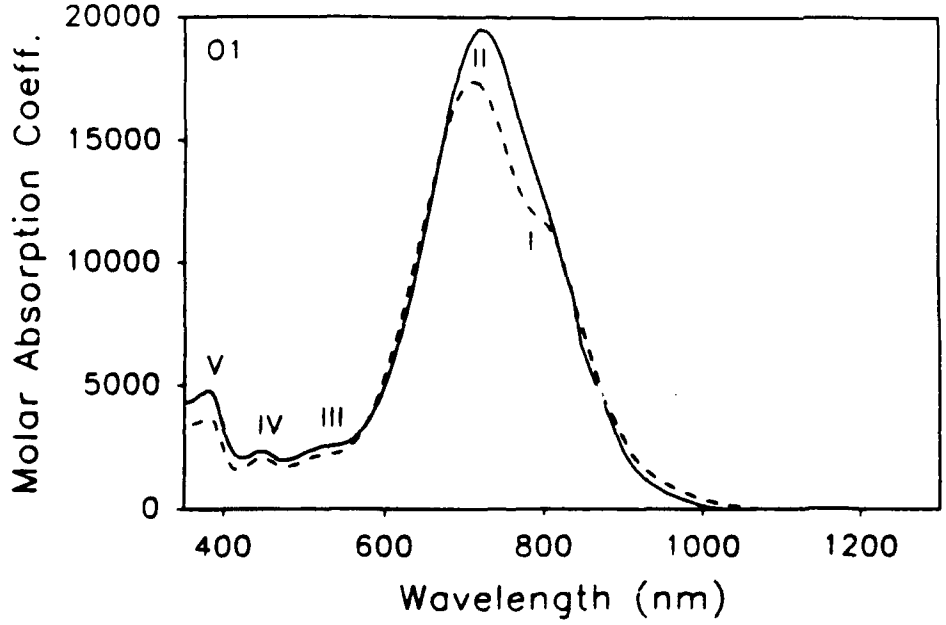
20000
15000
10000
5000
0
Molar Absorption Coeff.
01
V
IV
III
II
I
400
600
800
1000
1200
Wavelength (nm)

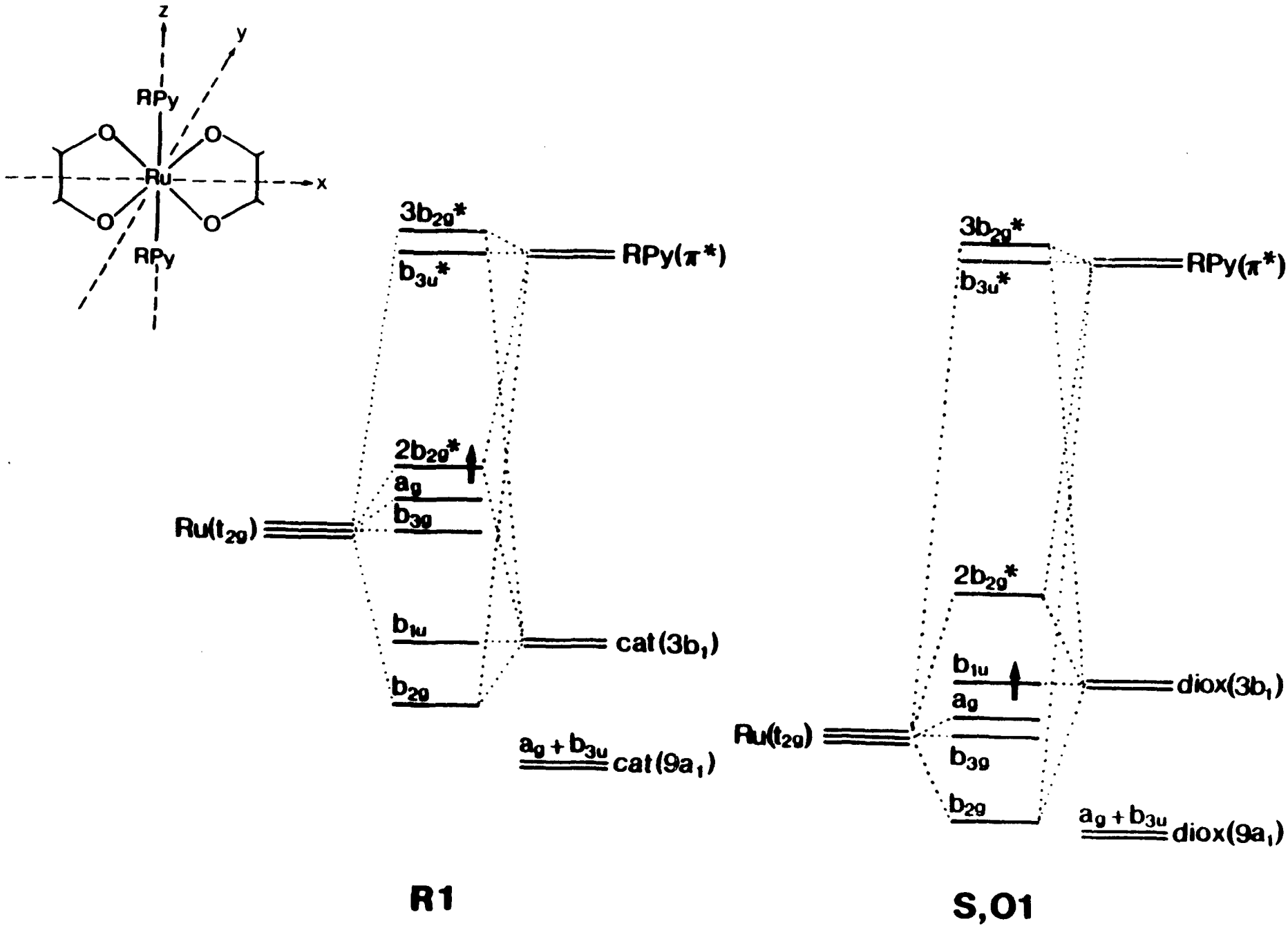
z
y
x
RPy
RPy
O
O
O
O
Ru
3b2g*
b3u*
2b2g*
ag
b3g
b1u
b2g
RPy(π*)
cat(3b1)
ag + b3u
cat(9a1)
Ru(t2g)
R1
3b2g*
b3u*
2b2g*
b1u
ag
b3g
b2g
RPy(π*)
diox(3b1)
ag + b3u
diox(9a1)
Ru(t2g)
S,O1

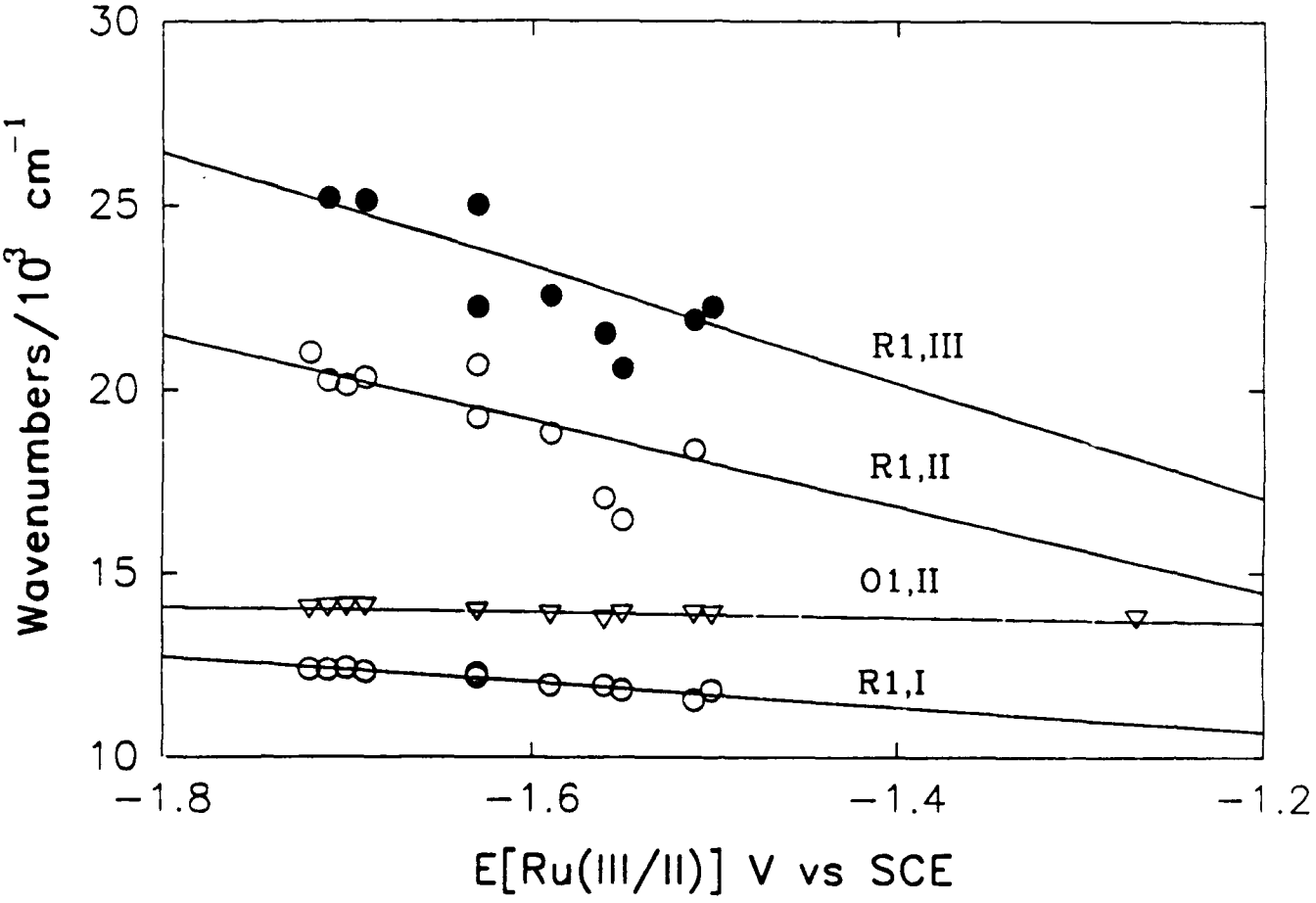
30
25
20
15
10
Wavenumbers/10^3 cm^{-1}
R1,III
R1,II
O1,II
R1,I
−1.8
−1.6
−1.4
−1.2
E[Ru(III/II)] V vs SCE

Supplementary Material

Table SI. Analytical Data for t-Ru(R-Py)$_2$(R'-Diox)$_2$, S, Complexes

		Anal. Calcd % (Found %)		
	Yield %	C	H	N
Ru(3-AcPy)$_2$(DTBDiox)$_2$	21	64.34(64.06)	6.96(7.05)	3.57(3.42)
Ru(4-AcPy)$_2$(DTBDiox)$_2$	25	64.34(64.10)	6.96(6.85)	3.57(3.61)
Ru(3-ClPy)$_2$(DTBDiox)$_2$	20	59.37(59.17)	6.29(6.29)	3.64(3.61)
Ru(4-ClPy)$_2$(DTBDiox)$_2$	13	59.37(59.22)	6.29(6.32)	3.64(3.65)
Ru(3-PhPy)$_2$(DTBDiox)$_2$	12	70.47(69.52)	6.86(6.69)	3.29(3.30)
Ru(Py)$_2$(DTBDiox)$_2$	40	65.20(64.84)	7.20(7.16)	4.00(3.99)
Ru(4-PhPy)$_2$(DTBDiox)$_2$	10	70.47(68.40)	6.86(6.58)	3.29(3.23)
Ru(4-VPy)$_2$(DTBDiox)$_2$	15	67.00(66.55)	7.23(7.24)	3.72(3.71)
Ru(4-MePy)$_2$(DTBDiox)$_2$	17	66.00(65.89)	7.48(7.55)	3.85(3.86)
Ru(3-EtPy)$_2$(DTBDiox)$_2$	14	66.72(66.47)	7.73(7.62)	3.70(3.71)
Ru(4-EtPy)$_2$(DTBDiox)$_2$	19	66.72(66.83)	7.73(7.73)	3.70(3.73)
Ru(4-BuPy)$_2$(DTBDiox)$_2$	25	68.03(68.21)	8.19(8.24)	3.45(3.41)
Ru(3-ClPy)$_2$(TBDiox)$_2$	22	54.88(54.94)	4.91(5.06)	4.27(4.32)
Ru(4-PhPy)$_2$(TBDiox)$_2$	22	68.16(67.93)	5.68(5.71)	3.79(3.80)
Ru(4-VPy)$_2$(TBDiox)$_2$	24	63.83(63.50)	5.99(5.89)	4.38(4.44)
Ru(4-BuPy)$_2$(TBDiox)$_2$.2H$_2$O	20	62.02(63.08)	7.40(7.06)	3.81(4.00)
Ru(4-BuPy)$_2$(MeDiox)$_2$	31	62.43(62.55)	6.22(6.45)	4.55(4.55)
Ru(4-BuPy)$_2$(Diox)$_2$	29	61.31(60.32)	5.83(5.88)	4.77(4.65)
Ru(4-BuPy)$_2$(ClDiox)$_2$	20	54.88(54.99)	4.91(5.00)	4.27(4.34)

Table SII. Analytical Data for t-[Ru(R-Py)$_2$(R'-Diox)$_2$]$^+$, **01**, Salts

	Anal. Calcd % (Found %)		
	C	H	N
[Ru(3-AcPy)$_2$(DTBDiox)$_2$]PF$_6$.CH$_2$Cl$_2$	50.93(50.99)	5.56(5.43)	2.76(2.88)
[Ru(4-AcPy)$_2$(DTBDiox)$_2$]PF$_6$.½CH$_2$Cl$_2$	52.54(52.63)	5.71(5.55)	2.88(2.94)
[Ru(3-ClPy)$_2$(DTBDiox)$_2$]ClO$_4$.½H$_2$O	52.03(51.91)	5.63(5.49)	3.19(3.19)
[Ru(3-ClPy)$_2$(DTBDiox)$_2$]PF$_6$.H$_2$O	48.98(48.75)	5.41(5.28)	3.00(2.97)
[Ru(3-ClPy)$_2$(DTBDiox)$_2$]SO$_3$CF$_3$	51.03(50.41)	5.27(5.46)	3.05(2.93)
[Ru(4-ClPy)$_2$(DTBDiox)$_2$]PF$_6$.CH$_2$Cl$_2$	46.90(46.69)	5.04(4.85)	2.80(2.79)
[Ru(3-PhPy)$_2$(DTBDiox)$_2$]PF$_6$.¼CH$_2$Cl$_2$	59.27(59.64)	5.79(5.78)	2.75(2.82)
[Ru(Py)$_2$(DTBDiox)$_2$]PF$_6$	54.02(53.92)	5.96(5.94)	3.31(3.26)
[Ru(4-PhPy)$_2$(DTBDiox)$_2$]SO$_3$CF$_3$	61.18(60.73)	5.83(5.88)	2.80(2.94)
[Ru(4-VPy)$_2$(DTBDiox)$_2$]PF$_6$.CH$_2$Cl$_2$	52.60(52.85)	5.75(5.91)	2.85(2.85)
[Ru(4-MePy)$_2$(DTBDiox)$_2$]ClO$_4$.CH$_2$Cl$_2$	53.98(54.53)	6.18(6.23)	3.07(3.19)
[Ru(3-EtPy)$_2$(DTBDiox)$_2$]PF$_6$.½CH$_2$Cl$_2$	54.10(53.67)	6.30(6.27)	2.97(2.86)
[Ru(4-EtPy)$_2$(DTBDiox)$_2$]PF$_6$.3CH$_2$Cl$_2$	46.76(47.38)	5.58(5.85)	2.42(2.64)
[Ru(4-BuPy)$_2$(DTBDiox)$_2$]SO$_3$CF$_3$.¼CH$_2$Cl$_2$	57.76(57.62)	6.83(6.85)	2.85(2.93)
[Ru(3-ClPy)$_2$(TBDiox)$_2$]PF$_6$.½CH$_2$Cl$_2$	43.39(43.41)	3.94(3.96)	3.31(3.37)
[Ru(4-VPy)$_2$(TBDiox)$_2$]PF$_6$.½CH$_2$Cl$_2$	50.09(50.21)	4.75(4.88)	3.12(3.34)

Table SIII. FTIR Data for t-Ru(RPy)$_2$(R'Diox)$_2$, S, Complexes[a]

Complex	Major Absorption Bands cm^{-1}
Ru(3-AcPy)$_2$(DTBDiox)$_2$	1695vs, 1595m, 1582w, 1533w, 1519m, 1464(Nujol), 1425w, 1377(Nujol), 1359s, 1293m, 1267s, 1212m, 1190w, 1159vs, 1103s, 1054m, 1025m, 990m, 960w, 910m, 865w, 822w, 749m, 700m, 655w
Ru(4-AcPy)$_2$(DTBDiox)$_2$	1699vs, 1583w, 1530m, 1517m, 1458w, 1420m, 1384m, 1376s, 1359s, 1294m, 1263s, 1212w, 1150vs, 1098s, 1060w, 1021m, 989w, 909w, 854w, 844w, 747w, 699m, 654w, 596m, 535w, 508s, 447w
Ru(3-ClPy)$_2$(DTBDiox)$_2$	1581m, 1530m, 1518m, 1462m, 1421w, 1375s, 1358s, 1295m, 1273w, 1245w, 1212w, 1147vs, 1095vs, 1048w, 1022m, 990w, 908m, 855w, 746m, 698m, 655w, 593w, 580w, 536m, 507s, 451m
Ru(4-ClPy)$_2$(DTBDiox)$_2$	1591s, 1532m, 1520m, 1460(Nujol), 1414m, 1377(Nujol), 1358s, 1295m, 1271w, 1246w, 1211m, 1203m, 1159vs, 1114m, 1100m, 1053m, 1023m, 992m, 912m, 849m, 823w, 750w, 733s, 699w
Ru(3-PhPy)$_2$(DTBDiox)$_2$	1583w, 1530m, 1517w, 1464(Nujol), 1456s, 1414w, 1374(Nujol), 1358m, 1295m, 1212w, 1154vs, 1100s, 1023w, 991w, 911w, 857w, 754m, 698m, 655w
Ru(Py)$_2$(DTBDiox)$_2$	1602m, 1578m, 1528m, 1516m, 1481w, 1452m, 1429w, 1375s, 1358s, 1311w, 1290m, 1253w, 1211m, 1144vs, 1101s, 1064w, 1022m, 987w, 908m, 853w, 739w, 675w, 577w, 529m, 504m, 446w.
Ru(4-PhPy)$_2$(DTBDiox)$_2$	1619s, 1583m, 1530m, 1514w, 1482m, 1463(Nujol), 1457s, 1424w, 1375(Nujol), 1359s, 1294m, 1273w, 1247w, 1214m, 1151vs, 1101s, 1024m, 992m, 958w, 911m, 855m, 768m, 748m, 699m, 654w, 628w
Ru(4-VPy)$_2$(DTBDiox)$_2$	1613m, 1582w, 1528m, 1458w, 1430w, 1384m, 1374m, 1358m, 1293m, 1212w, 1140vs, 1099s, 1023m, 991m, 910m, 854w, 747m, 696m, 537w, 509m, 450m

Ru(4-MePy)$_2$(DTBDiox)$_2$ 1618m, 1584m, 1530s, 1516m, 1502w, 1460w, 1429w, 1375s, 1356s, 1294m, 1272w, 1246w, 1211m, 1148vs, 1099s, 1021m, 990m, 910m, 859w, 816w, 747m, 697m, 596w, 577w, 535s, 509s, 449m

Ru(3-EtPy)$_2$(DTBDiox)$_2$ 1601w, 1579m, 1527m, 1510m, 1464(Nujol), 1374(Nujol), 1359s, 1316m, 1295s, 1275w, 1245m, 1216m, 1148vs, 1102s, 1063w, 1053w, 1025m, 991m, 942w, 910s, 855m, 811w, 747w, 701m, 659w

Ru(4-EtPy)$_2$(DTBDiox)$_2$ 1617m, 1584m, 1530s, 1516m, 1464(Nujol), 1457s, 1432m, 1375(Nujol), 1356m, 1321w, 1294s, 1273m, 1246m, 1212w, 1191w, 1154vs, 1100s, 1068w, 1022s, 990m, 962w, 911m, 858m, 836w, 748m, 700m, 654w

Ru(4-BuPy)$_2$(DTBDiox)$_2$ 1583m, 1540w, 1521m, 1480w, 1458m, 1429w, 1384s, 1361s, 1291m, 1214w, 1168vs, 1148s, 1097s, 1025s, 985m, 909m, 856w, 742w, 695w, 655w, 530m, 503s

Ru(3-ClPy)$_2$(TBDiox)$_2$ 1577m, 1522s, 1463(Nujol), 1435s, 1401s, 1377(Nujol), 1317s, 1257m, 1214s, 1161vs, 1125vs, 1108s, 1025m, 861m, 807m, 649m

Ru(4-PhPy)$_2$(TBDiox)$_2$ 1611m, 1576m, 1539w, 1523m, 1507w, 1466(Nujol), 1457vs, 1449s, 1440s, 1401m, 1377(Nujol), 1365w, 1322w, 1311w, 1260w, 1210m, 1168s, 1124s, 1111m, 1019w, 1011w, 959w, 837m, 802m, 768m, 732m, 727m, 720m, 693w, 689w, 651m, 629m, 538m, 534m, 508m, 501w

Ru(4-VPy)$_2$(TBDiox)$_2$ 1610m, 1577m, 1570m, 1546w, 1540w, 1521m, 1507w, 1457w, 1437s, 1415w, 1400s, 1386w, 1362m, 1314m, 1258m, 1212m, 1170s, 1158s, 1123s, 1107s, 1083w, 1022m, 987w, 935w, 863m, 804m, 692w, 676w, 668w, 652m, 644m, 631m, 576w, 536s, 516w

---

a. Samples were run as KBr disks or Nujol mulls on KBr or NaCl plates.

b. Relative intensities: (v)s = (very) strong, m = medium, w = weak.

Table SIV. FTIR Data for t-[Ru(RPy)$_2$(R'Diox)$_2$]$^+$, O1, Salts

Complex	Major Absorption Bands cm^{-1}
[Ru(3-AcPy)$_2$(DTBDiox)$_2$]PF$_6$	1701s, 1604m, 1576m, 1520m, 1507m, 1464(Nujol), 1458s, 1376(Nujol), 1364m, 1341w, 1273m, 1241m, 1197w, 1091m, 1057w, 1027m, 988m, 905w, 846vs(PF$_6$), 695m, 656w
[Ru(4-AcPy)$_2$(DTBDiox)$_2$]PF$_6$	1700vs, 1576m, 1523m, 1514m, 1507m, 1458vs, 1419s, 1377(Nujol), 1366s, 1348m, 1261s, 1242m, 1214w, 1092m, 1056m, 1028m, 988m, 966w, 906w, 878m, 848vs(PF$_6$), 836vs(PF$_6$), 778w, 750w, 738w, 727w, 721w, 659w, 603m, 597m, 558s(PF$_6$), 510m, 501m
[Ru(3-ClPy)$_2$(DTBDiox)$_2$]PF$_6$	1577m, 1540w, 1507m, 1464(Nujol), 1457s, 1418m, 1376(Nujol), 1367m, 1350m, 1329w, 1258m, 1240m, 1197w, 1126m, 1089m, 1062m, 1027m, 987m, 904m, 846vs(PF$_6$), 812m, 782w, 758w, 743m, 694m, 557s, 515m, 493m
[Ru(4-ClPy)$_2$(DTBDiox)$_2$]PF$_6$	1600vs, 1576m, 1521m, 1507m, 1481w, 1465(Nujol), 1457s, 1424m, 1377(Nujol), 1366m, 1349m, 1260w, 1242m, 1213w, 1118m, 1090m, 1057m, 1030m, 989m, 905m, 869m, 839vs(PF$_6$), 827vs(PF$_6$), 780w, 740s, 558s(PF$_6$), 509w, 495s
[Ru(3-PhPy)$_2$(DTBDiox)$_2$]PF$_6$	1572m, 1507m, 1464(Nujol), 1457vs, 1416m, 1376(Nujol), 1365m, 1349w, 1243m, 1200w, 1195w, 1091m, 1032w, 1014w, 991m, 908m, 874w, 848vs(PF$_6$), 831vs(PF$_6$), 774w, 759s, 720w, 700s
[Ru(Py)$_2$(DTBDiox)$_2$]PF$_6$	1608m, 1577m, 1521m, 1507m, 1464(Nujol), 1457vs, 1437m, 1385m, 1375(Nujol), 1363m, 1339m, 1299w, 1262w, 1239m, 1213w, 1092m, 1068m, 1028m, 987m, 906m, 875m, 839vs(PF$_6$), 766w, 697m, 557s(PF$_6$), 505m
[Ru(4-PhPy)$_2$(DTBDiox)$_2$]SO$_3$CF$_3$	1615s, 1577m, 1507m, 1463(Nujol), 1423m, 1377(Nujol), 1365m, 1347w, 1291m(SO$_3$CF$_3$), 1272s(SO$_3$CF$_3$), 1265s(SO$_3$CF$_3$),

1240s(SO_3CF_3), 1221m(SO_3CF_3), 1158s(SO_3CF_3), 1090m, 1078m, 1069m, 1029s(SO_3CF_3), 1013w, 987m, 905w, 864w, 853w, 830w, 767m, 728w, 691w, 659w, 637s(SO_3CF_3), 631m(SO_3CF_3), 515m, 500m

[Ru(4-VPy)$_2$(DTBDiox)$_2$]PF$_6$ 1616vs, 1576m, 1522m, 1507s, 1458vs, 1435m, 1418w, 1377(Nujol), 1365w, 1349w, 1242m, 1207s, 1092m, 1066w, 1027m, 1000w, 989m, 933w, 906m, 872m, 851vs(PF_6), 839vs(PF_6), 779m, 732m, 558s(PF_6), 500m

[Ru(4-MePy)$_2$(DTBDiox)$_2$]ClO_4 1619s, 1577m, 1520m, 1506m, 1463m, 1442m, 1364m, 1349m, 1298w, 1242m, 1211m, 1093vs (ClO_4), 1064w, 1040m, 1029m, 989m, 905w, 860m, 829w, 819m, 780w, 750w, 695w, 623s(ClO_4), 515w, 494s

[Ru(3-EtPy)$_2$(DTBDiox)$_2$]PF$_6$ 1604w, 1577m, 1507m, 1480m, 1465(Nujol), 1457s, 1437m, 1376(Nujol), 1365m, 1354m, 1260w, 1240m, 1192w, 1118w, 1090m, 1063w, 1026m, 987m, 905w, 850vs(PF_6), 844vs(PF_6), 783w, 738m, 703m, 661m, 558s(PF_6), 516w, 496m

[Ru(4-EtPy)$_2$(DTBDiox)$_2$]PF$_6$ 1617m, 1576m, 1522m, 1517m, 1507m, 1465(Nujol), 1458s, 1436m, 1377(Nujol), 1365m, 1349w, 1340w, 1242m, 1215w, 1092m, 1066w, 1038w, 1030m, 989m, 906w, 877m, 847vs(PF_6), 838vs(PF_6), 779w, 732w, 558s(PF_6), 496m

[Ru(4-BuPy)$_2$(DTBDiox)$_2$]SO_3CF_3 1615m, 1576m, 1464(Nujol), 1426m, 1376(Nujol), 1367m, 1346w, 1275vs(SO_3CF_3), 1241m(SO_3CF_3), 1220m(SO_3CF_3), 1144s(SO_3CF_3), 1092m, 1071m, 1033s(SO_3CF_3), 987m, 906w, 861w, 838w, 827w, 750w, 722w, 638s(SO_3CF_3), 514m, 501m

[Ru(3-ClPy)$_2$(TBDiox)$_2$]ClO_4 1576m, 1501s, 1463(Nujol), 1378(Nujol), 1317w, 1243m, 1201m, 1093vs(ClO_4), 1026m, 813m, 723m, 688m

[Ru(4-PhPy)$_2$(TBDiox)$_2$]PF$_6$ 1616s, 1575m, 1506m, 1500m, 1498m, 1466(Nujol), 1462s, 1457vs, 1448m, 1440w, 1421w, 1379(Nujol), 1371m, 1237m, 1231w, 1072m, 1017w, 1011w, 853s(PF_6), 837vs(PF_6), 765m, 727m, 686m, 631m, 558m(PF_6), 509m, 500m, 493m

[Ru(4-VPy)$_2$(TBDiox)$_2$]PF$_6$ 1616vs, 1576m, 1570m, 1506m, 1498s, 1465(Nujol), 1457vs, 1448m, 1437m, 1418m, 1375(Nujol), 1367m, 1354w, 1289w, 1241m, 1226m, 1204m, 1148w, 1071m, 1024m, 998w, 992w, 934w, 874m, 840vs(PF$_6$), 798w, 724w, 641m, 558s(PF$_6$), 501m, 473m

---

a. Samples were run as Nujol mulls on KBr or NaCl plates. Where Nujol peaks are not reported, the data were also collected in HCBD.

b. Relative intensities: (v)s = (very) strong, m = medium, w = weak.